A light-emitting-diode pulsing system for measurement of time-resolved luminescence

by

Solomon Akpore Uriri

supervised by

Professor Makaiko L. Chithambo

A thesis submitted to the Department of Physics and Electronics, Faculty of Science, Rhodes University, in fulfilment of the requirements for the degree of Master of Science

February 20, 2015

Abstract

A new light-emitting-diode based pulsing system for measurement of time-resolved luminescence has been developed. The light-emitting-diodes are pulsed at various pulse-widths by a 555-timer operated as a monostable multivibrator. The light-emitting-diodes are arranged in a dural holder connected in parallel in sets of four, each containing four diodes in series. The output pulse from the 555-timer is fed into an 2N7000 MOSFET to produce a pulse-current of 500 mA to drive the set of 16 light-emitting-diodes. This size of current is sufficient to drive the diodes with each driven at a pulse-current of 90 mA with a possible maximum of 110 mA per diode. A multichannel scaler is used to trigger the pulsing system and to record data at selectable dwell times. The system is capable of generating pulse-widths in the range of microseconds upwards. The new pulsing system was used to study the dependence of luminescence lifetimes on radiation dose and, on measurement temperature in quartz and α-Al_2O_3:C. In quartz, lifetimes measured between 5 and 200 Gy beta dose were constant at about 42.0 $\pm$ 1.3 μs. On the other hand, the lifetimes decreased with measurement temperature from 40.4 $\pm$ 0.9 μs at 20 ^{0}C to 14.8 $\pm$ 1.8 μs at 200 ^{0}C. In α-Al_2O_3:C, luminescence lifetimes decreased from 36.8 $\pm$ 0.1 ms at 20 ^{0}C to 28.0 $\pm$ 0.6 ms at 140 ^{0}C. The dependence of luminescence lifetimes on measurement temperature in quartz and α-Al_2O_3:C showed evidence of thermal quenching at high temperature. Thermal quenching is the decrease of luminescence due to increased non-radiative transitions at high temperature. The value of the activation energy for thermal quenching for quartz was evaluated as 0.67 $\pm$ 0.05 eV and as 1.02 $\pm$ 0.01 eV for α-Al_2O_3:C.

Acknowledgements

"Genius is one percent inspiration, ninety-nine percent perspiration."

— *Thomas A. Edison*

I am indeed grateful to the Almighty God for the gift of life and for giving me the best supervisor. I would like to express my profound appreciation to my supervisor Prof. Makaiko L. Chithambo whose fatherly care, constructive criticisms, suggestions, patience and inestimable assistance, enhanced the quality of this research study. May the Almighty God continue to guide, protect and uplift you in all manners of life. My sincere gratitude also goes to Mr Andy Youthed for providing technical advice. Your valuable inputs transcended beyond all reasonable measures.

Special thanks to my parents Overseer & Deaconess John Uriri for their constant encouragement, support, care and prayers during the course of this project. Many thanks to my only dearest brother, Dr. Nelson Oghenekaro Odume for taking time to proof read the first manuscript of this project and being my major motivator in life. To my love Favour Omenuwoma Owhe, my deepest gratitude for your love, understanding, care and prayers you shown to me all through till the end of this project.

I would like to thank the National Research Foundation of South Africa for providing financial support in form of scholarship through the Innovation bursary scheme (grant number: 90451) and for sponsoring my travel trip to attend South African Institute of Physics 2014 annual conference. To Rhodes University, I say thank you for providing a conducive research environment in form of laboratories, wonderful staff and science equipment that made this project possible. The university refined me into a growing and a professional physics scholar. Indeed, you are really the "smallest university where leaders learn".

I must not forget to acknowledge staff of the Physics and Electronics Department, my fellow colleagues and friends for the wonderful time we had together. God bless you all!!!

Dedication

I dedicate this project to my parents Overseer & Deaconess John Uriri. Your endless motivation, love, support inspired me to accomplish this work.

Contents

List of Figures

List of Tables

Chapter 1

1.1 Luminescence

Luminescence is the process by which light of a certain wavelength is emitted from previously irradiated materials, mostly insulators and semiconductors when heated or under exposure to light at a different wavelength. The source of the ionizing radiation can be beta, alpha, X-ray or gamma radiation as well as ultraviolet light. The absorption of energy from the ionising radiation produces free electrons and holes. These free charges are subsequently trapped at point-defects within the material [1]. In the case of electrons, such defects are called electron traps whereas for holes, they are called hole traps.

During exposure to light (a process called optical stimulation), the trapped electrons are released from the traps back into the conduction band. The electrons may then recombine with charge carriers of opposite sign at a recombination centre. If the recombination is radiative, light at a different wavelength is emitted. This emitted light is called luminescence.

In general, the trapped electrons can be stimulated optically or thermally. Optical stimulation is achieved if the material is exposed to light of a certain wavelength, say 470 nm blue light. The resulting luminescence is called optically stimulated luminescence (OSL). If the material is heated under a controlled heating rate, the luminescence is called

thermoluminescence (TL) [2].

Figure 1.1 shows the processes leading up to emission of optically stimulated luminescence (OSL) and thermoluminescence (TL). The figure is divided into three stages namely; (i) ionisation, (ii) storage of radiation energy in time and (iii) eviction in (A) and recombination in (B). Each stage is separated by dashed vertical lines. In part (i) some electrons get excited into the conduction band due to exposure to irradiation leaving a hole in the valence band. The electrons are trapped at the electron trap labelled T and the holes trapped at a hole trap labelled L. The parameter E is the energy depth of the trap below the conduction band [3]. By heating or shining light onto the sample, electrons are evicted from the electron traps and some of these reach luminescence centres also referred to as the recombination centre. OSL or TL is emitted during the process of recombination as represented in part (iii)(B) in the figure.

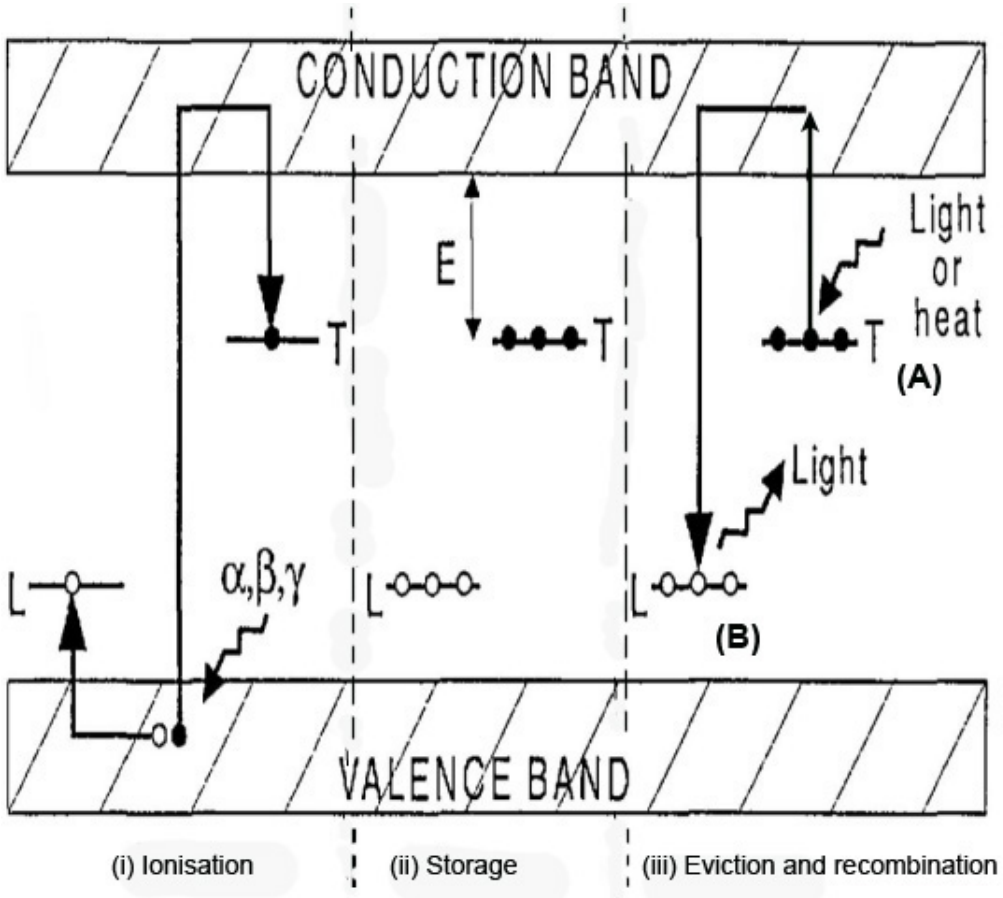

Figure 1.1: Energy-level representation showing the three stages of TL and OSL processes indicated as (i) ionisation, (ii) storage and (iii) eviction and recombination. The processes are shown by dashed vertical-lines [4].

1.1.1 Types of luminescence

The names given to various luminescence phenomena reflect the type of radiation used to excite the charges. Thus, luminescence is classified as photoluminescence (excitation by optical or ultraviolet light), radioluminescence (caused by nuclear radiation such as gamma-rays or X-rays) and cathodoluminescence (caused by an electron beam). Luminescence can also be emitted due to chemical energy (chemiluminescence), biochemical energy (bioluminescence), mechanical energy (triboluminescence), electrical energy (electroluminescence) and sound waves (sonoluminescence).

Luminescence can be sub-classified into fluorescence or phosphorescence based on the time τ_e after which the emission of light takes place after irradiation. If the emission occurs some time $\tau_e < 10^{-8}$ s, it is called fluorescence. On the other hand, if the emission occurs some time $\tau_e > 10^{-8}$ s, it is called phosphorescence.

Fluorescence is the spontaneous emission of luminescence after exposure of the material to irradiation. Figure 1.2 illustrates the basic process responsible for fluorescence. After irradiation energy is absorbed, electrons are excited from the ground state g to an excited energy state e. Light is emitted when electrons relax from the excited state e to the ground state g.

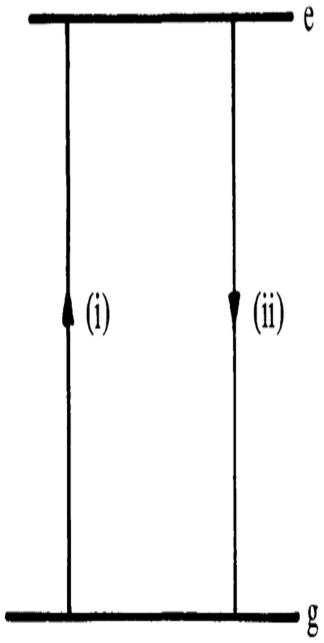

Figure 1.2: Transitions involved in the production of fluorescence. Transition (i) shows the excitation of electrons from the ground state g to an excited energy state e. Transition (ii) shows the relaxation of an excited electron back to the ground state g during which light is emitted [3].

Phosphorescence is preceded by a delay between the irradiation and the time t_{max} to reach maximum intensity. Figure 1.3 shows the energy transitions involved in the process of phosphorescence. In comparison with figure 1.2, the energy diagram of figure 1.3 includes

an additional metastable state m (an energy E below level e) where the electrons may transit into and out of to an excited state e before decaying back to the ground state g. The delay between the excitation and emission of phosphorescence occurs because it involves the transition into and out of the metastable state m. Hence, the delay time τ_e is greater than 10^{-8} s. If the delay is of the order of 1 second, it is easy to categorize the emission as phosphorescence but when the delay time τ_e between excitation and emission is much shorter than 1 second, it becomes difficult to distinguish between fluorescence and phosphorescence [3]. Fluorescence is temperature independent whereas phosphorescence is strongly dependent on temperature [3].

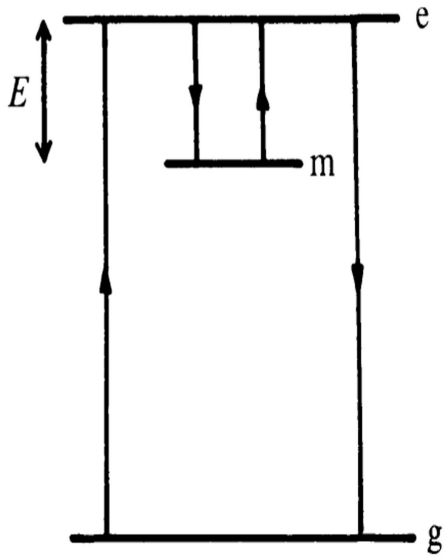

Figure 1.3: Energy transitions involved in the process of phosphorescence.

1.2 Defects in solids

Some of the free electrons produced due to ionising radiation are trapped at point-defects in the material as illustrated for phosphorescence in Figure 1.3. Defects in crystalline solids often influence their physical properties including optical absorption or emission; mechanical, magnetic, and electrical properties. Defects in crystalline solids occur as a result of disorder in the crystal structure or due to presence of impurities. There are many

types of point-defect including impurities, interstitials and vacancies. Point-defects occur at or around a single lattice point and can be intrinsic or extrinsic. The displacement of an atom within the crystalline lattice produces intrinsic defects whereas extrinsic defects are caused by impurities in the crystalline solid. For example, an interstitial is a position not normally occupied by an atom in the crystal lattice. Another example, a vacancy, is created by a missing atom in the crystalline lattice.

1.3 Optically stimulated luminescence

This section explains the basic theory of optically stimulated luminescence (OSL). Optically stimulated luminescence is the luminescence emitted at one wavelength from an irradiated insulator or semiconductor when exposed to light at a different wavelength. Figure 1.4 shows a schematic representation of an OSL process. The radiation creates, by ionisation, free electrons and holes. The electrons or holes can subsequently be trapped at point-defects in the crystal lattice. The material may then be stimulated with light of a particular wavelength to release trapped electrons which thereafter transit from the trap into the conduction band. Luminescence is emitted during radiative recombination of electrons and holes at a recombination centre. However, non-radiative recombination may also occur whereby the absorbed energy is released as phonons.

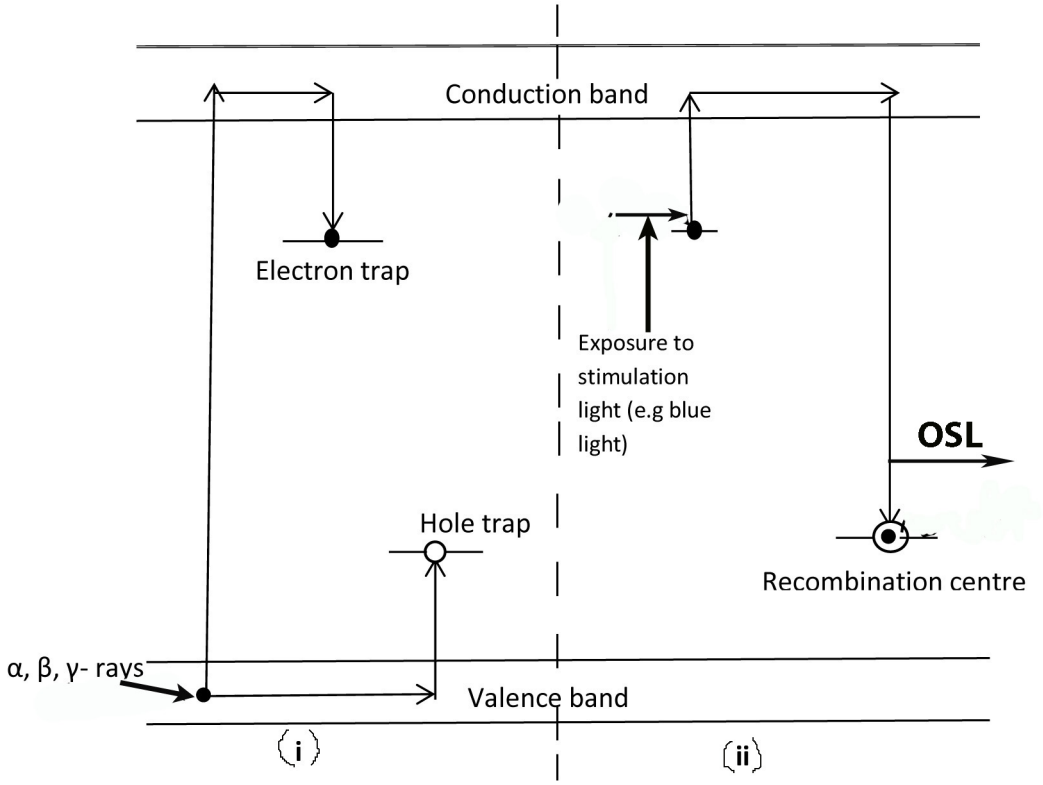

Figure 1.4: A schematic diagram showing the OSL process. Part (i) shows the excitation of electrons into the conduction band by irradiation and the trapping of an electron and a hole at point defects. Part (ii) shows the transition of a trapped electron back into the conduction band due to optical stimulation, and recombination with charge of opposite sign (a hole) at the recombination center during which OSL is emitted.

1.3.1 Measurement of optically stimulated luminescence

Optically stimulated luminescence measurements are carried out by the stimulation of an irradiated sample with a light source emitting visible, ultra-violet or infrared light at a certain wavelength. The luminescence emitted from the sample at a different wavelength is monitored using a sensitive light detector, usually a photomultiplier tube.

There are three types of optically stimulated luminescence. These are continuous-wave optically stimulated luminescence (CW-OSL), linear-modulation optically stimulated luminescence (LM-OSL) and pulsed optically stimulated luminescence (POSL) also known as time-resolved optically stimulated luminescence (TR-OSL).

1.3.1.1 Continuous-wave OSL

Continuous-wave optical stimulation of luminescence is the process whereby an irradiated sample is illuminated with light at constant intensity and the emitted luminescence monitored simultaneously with the stimulating light. In this case, the luminescence and stimulating light are discriminated by wavelength separation (i.e the OSL emission wavelength λ_{OSL} not being equal to the stimulation wavelength λ_{stim}) [5]. To achieve this, a bandpass filter is placed in front of the stimulation light source and a transmission filter in front of the photomultiplier tube to prevent scattered light from the stimulation source from reaching the photomultiplier tube. As an example, a Schott GG-420 bandpass filter can be placed in front of 470 nm blue LEDs and a Hoya U340 transmission filter located in front of a photomultiplier tube [6, 7].

The luminescence emitted under CW-OSL is monitored as a function of time resulting in a luminescence-versus-time curve known as a decay curve. Figure 1.5 is a schematic representation of measurement of CW-OSL. The stimulation is done at constant intensity denoted by the horizontal line with respect to time. The inset shows an example of a decay curve obtained from a sample of natural quartz after beta irradiation to 20 Gy. The CW-OSL was measured at 20^0C with blue light-emitting-diodes used as the stimulating light source.

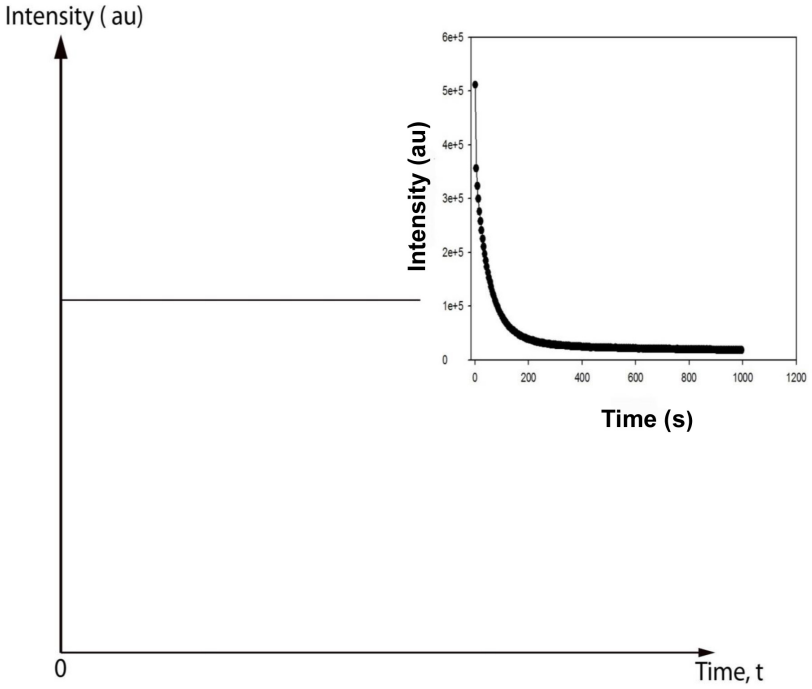

Figure 1.5: A schematic representation of CW-OSL as a function of time. The inset shows a CW-OSL decay curve obtained from a sample of natural quartz after beta irradiation to 20 Gy.

1.3.1.2 Linear-modulation OSL

Linear modulation optical stimulation of luminescence (LM-OSL) is the process whereby an irradiated sample is stimulated by a light source whose intensity is increased linearly in time. This method for measuring optically stimulated luminescence was introduced by Bulur [8]. Figure 1.6 shows a schematic representation of measurement of LM-OSL. The intensity is increased linearly as a function of time. The inset shows an example of an LM-OSL curve obtained from a sample of natural quartz after beta irradiation to 20 Gy. In LM-OSL, the graphs of OSL intensity against time are peak-shaped as shown in Figure 1.6 (inset). The peak corresponds to the optical release of charge from a particular trap. No peak is apparent after 800 seconds.

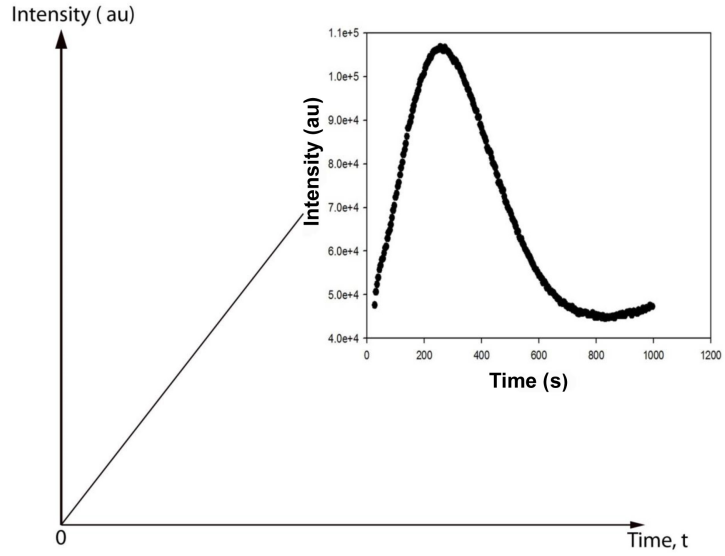

Figure 1.6: A schematic representation showing the linear increase of the stimulation intensity as a function of time. The inset shows an LM-OSL curve obtained from a sample of natural quartz after beta irradiation to 20 Gy.

1.3.1.3 Time-resolved optically stimulated luminescence

Time-resolved optically stimulated luminescence (TR-OSL) also known as pulsed optically stimulated luminescence is the luminescence observed when a sample is pulsed-stimulated at a selected pulse-width. A time-resolved spectrum consists of two portions, namely, the signal during stimulation and signal after stimulation. During stimulation, the signal observed consists of photomultiplier noise, scattered stimulation light and the luminescence build-up whereas after stimulation (i.e when the light is OFF), the luminescence observed consists of the photomultiplier noise and the measured luminescence only [9]. Thus, time-resolved optically stimulated luminescence separates in time the stimulation and emission of luminescence.

Systems for measurement of time-resolved optically stimulated luminescence based on laser and light-emitting-diodes have been described previously [10, 11, 12]. Sanderson and Clark [10] used 470 nm light from an N_2 dye laser to pulse OSL from alkali feldspar with a pulse-width of the order of 10 ns. Markey et al. [11] and Mckeever et al. [12] used

TR-OSL to study the features of luminescence from α-Al_2O_3 in which the light from an Ar-ion laser was used to stimulate luminescence. Chithambo and Galloway [13] used a pulsed 525 nm green light-emitting-diode system to stimulate luminescence from feldspar and quartz.

Figure 1.7 shows a schematic representation of a TR-OSL in (a) and an example of a TR-OSL spectrum in (b). The stimulation is performed using a brief light-pulse of duration t_w and period T for a dynamic range t as shown in (a). Figure 1.7 (b) shows an example of a TR-OSL spectrum obtained from a sample of quartz after beta irradiation to 120 Gy. TR-OSL was measured at 25 ^{0}C and stimulated at 11 μs [14].

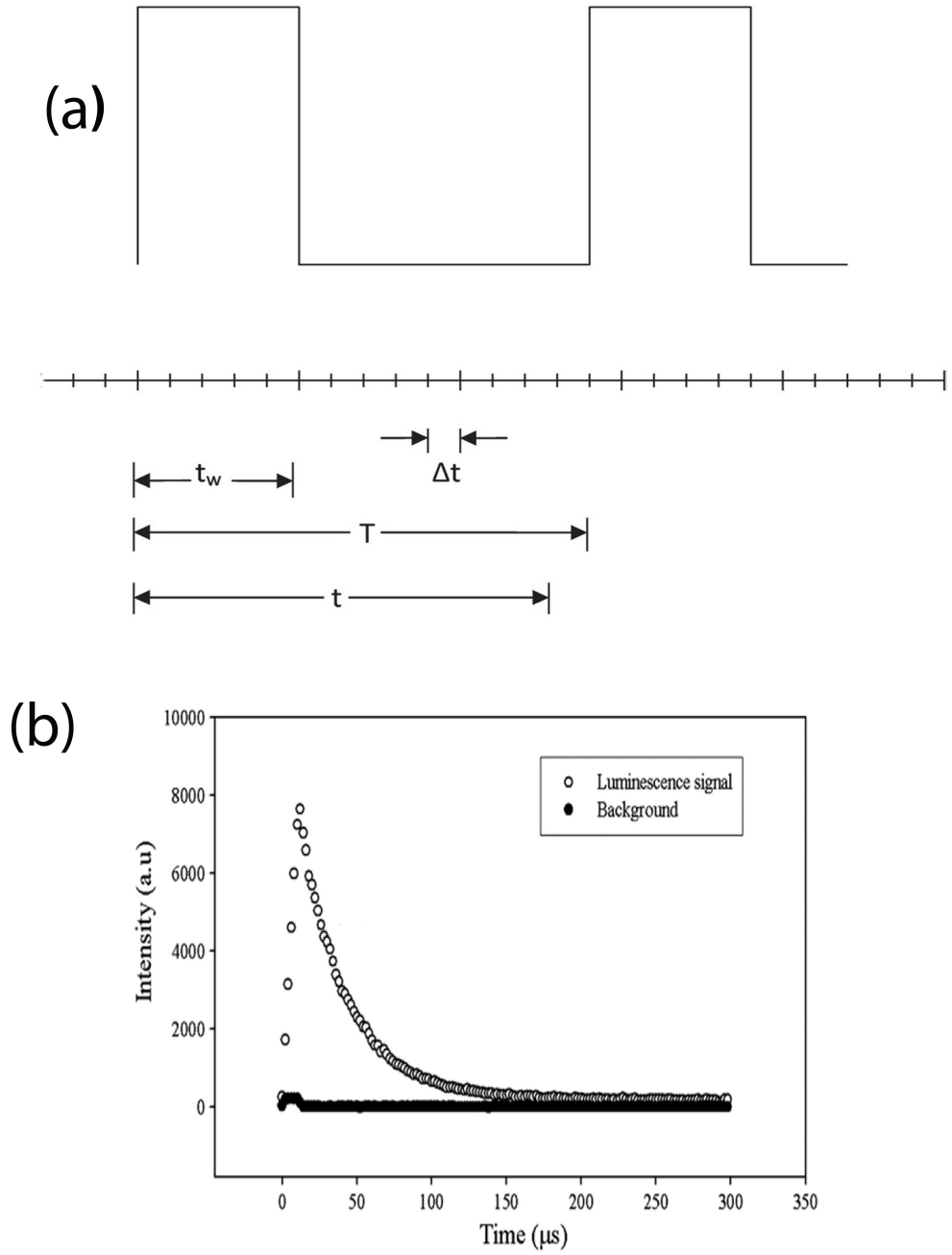

Figure 1.7: A schematic representation of TR-OSL stimulating light pulse of duration t_w and period T where the dynamic range t is subdivided into an integral number of $n\Delta t$ channels where Δt is the dwell time [9] (a). A TR-OSL spectrum from a sample of quartz irradiation to 120 Gy. The sample was stimulated using 470 nm blue LEDs at 11 μs per pulse (b) [14]. Figure 1.7 (a) has been reproduced from Chithambo [9].

1.4 Aim of the thesis

Time-resolved optically stimulated luminescence (TR-OSL) is used to study the mechanisms of luminescence in materials relevant to dosimetry. TR-OSL separates in time the stimulation and emission of luminescence. Luminescence lifetime is the delay between stimulation and emission of luminescence. Lifetimes enable the study of recombination in a material thereby providing important information on the underlying luminescence mechanisms [14, 15]. Measurement systems for TR-OSL based on laser and LED systems have been previously described for example, Markey et al. [11] used TR-OSL to study features of luminescence from α-Al_2O_3 in which the light from an Ar-ion laser was used to stimulate luminescence. Chithambo and Galloway [13] used a pulsed 525 nm green light-emitting-diode system to measure luminescence from feldspar and quartz.

The aim of this study was to develop a new light-emitting-diode based pulsing system for measurement of TR-OSL. This study was done to produce a system capable of automatic control of the stimulation power and able to produce a range of pulse-widths. The design of the pulsing circuitry is new and has been tested on quartz and α-Al_2O_3:C the luminescence dosimeters.

1.5 Synopsis of thesis

The remaining part of the thesis is organized as follows: Chapter 2 presents a generalised mathematical description of OSL. Chapter 3 focusses on the theory and analysis of time-resolved optically stimulated luminescence. Chapter 4 provides detailed information on the design and development of the new light-emitting-diode pulsing system. Chapter 5 presents the applications of the system to quartz and Al_2O_3:C, materials relevant to retrospective dosimetry. The summary of the design of the pulsing system and the applications of the system to quartz and α-Al_2O_3:C with recommendations for future studies are given

in Chapter 6. The appendices contain description of components used in the design of the pulsing system and an operation manual for the pulsing system.

Chapter 2

Optically stimulated luminescence

This chapter discusses a generalized mathematical description of optically stimulated luminescence (OSL).

Optically stimulated luminescence is obtained from irradiated materials during exposure to light. The OSL process involves two stages; namely, excitation by irradiation and, illumination. Following irradiation, free electrons and holes are created as a result of ionisation. The free electrons in the conduction band and free holes in the valence band may then be trapped at point-defects in the crystal lattice. The concentration of trapped electrons and that of holes is dependent on the absorbed dose of radiation.

After the excitation, the sample may then be illuminated, for example by a set of light-emitting-diodes of a certain wavelength. The light stimulates the release of the trapped electrons at point-defects back into the conduction band. The electrons may then transit through the conduction band and recombine with holes at the recombination centre. If the recombination is radiative, light is emitted. This type of process is called radiative recombination. Non-radiative recombination may also occur when the absorbed energy is released as phonons.

2.1 Types of optically stimulated luminescence

There are three techniques to optically stimulate luminescence from materials as previously mentioned in section 1.3.1. These are CW-OSL, LM-OSL, and TR-OSL. These stimulation types are classified according to how the stimulation light intensity is controlled during experiment.

2.1.1 Continuous-wave optically stimulated luminescence

Continuous-wave optically stimulated luminescence (CW-OSL) is a technique whereby an irradiated material is illuminated with light of constant intensity and the luminescence monitored simultaneously with stimulating light. The luminescence appears as a decay curve.

Figure 2.1 shows the processes involved in production of OSL. The figure shows the excitation of the OSL material by ionizing radiation to create free electrons and holes. These excited electrons and holes may then be trapped at electron traps and hole traps respectively. The trapped electrons are optically stimulated into the conduction band and then subsequently recombine with the trapped holes at the recombination centre to produce light otherwise referred to as OSL.

Consider a simple model involving one trap and one recombination centre as shown in Figure 2.1. Let n be the concentration of trapped electrons, n_c the concentration of electrons in the conduction band, A_n the trapping probability (in units of $\mathrm{m^3 s^{-1}}$), N the total available concentration of electron traps, m the concentration of trapped holes, A_m the recombination probability (in units of $\mathrm{m^3 s^{-1}}$) and M the total available concentration of hole traps.

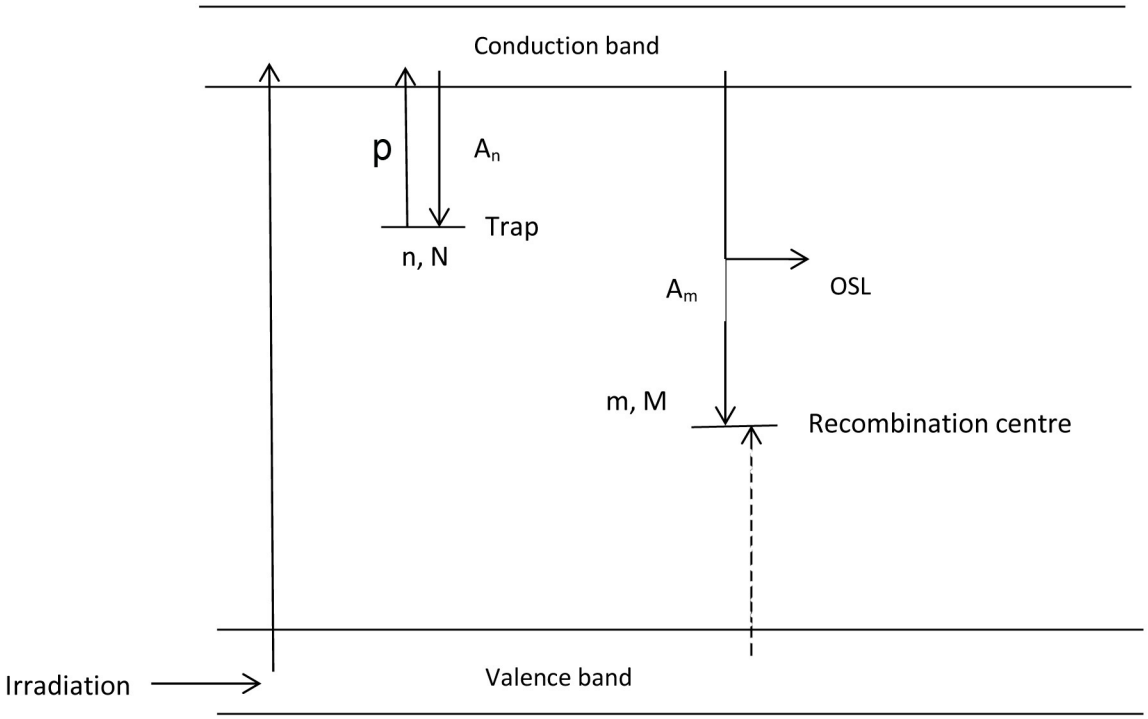

Figure 2.1: An OSL process that involves one trap and one recombination centre. The figure shows excitation by ionizing radiation creating free electrons and holes. The trapped electrons are optically stimulated from the trap into the conduction band and then subsequently recombine with the trapped holes at the recombination centre to produce OSL.

It should be noted that during optical stimulation, transitions of trapped electrons to the valence band does not occur. Thus, charge neutrality requires that

$$n_c + n = m. \tag{2.1}$$

We may then write the rate of change of the various concentrations as

$$\frac{dn_c}{dt} + \frac{dn}{dt} = \frac{dm}{dt}. \tag{2.2}$$

Re-arranging equation 2.2, we get

$$\frac{dn_c}{dt} = -\frac{dn}{dt} + \frac{dm}{dt}. \tag{2.3}$$

The rate of stimulation p of trapped electrons is related to the incident photon flux Φ and the photoionisation cross-section σ by

$$p = \Phi\sigma, \tag{2.4}$$

where p is in units of s^{-1}. The rate of change of the concentration of trapped electrons dn/dt can be written explicitly as

$$\frac{dn}{dt} = np - n_c A_n (N - n). \tag{2.5}$$

Equation 2.5 assumes the rate of change of concentration of trapped electrons is proportional to the concentration of electrons in the conduction band. The rate of change of concentration of holes in the valence band dm/dt can be written as

$$\frac{dm}{dt} = n_c A_m m = \frac{n_c}{\tau}. \tag{2.6}$$

Equation 2.6 assumes the recombination rate is proportional to the concentration of holes in the valence band. Assuming quasi-equilibrium, i.e when $\frac{dn_c}{dt} << \frac{dn}{dt}, \frac{dm}{dt}$ and $n_c << n, m$ we have, from equation 2.3, that

$$\frac{dm}{dt} \equiv \frac{dn}{dt}. \tag{2.7}$$

Also assuming slow-retrapping, that is if $n_c A_n (N - n) << np; n_c A_m m$; the OSL intensity I_{OSL} will be

$$I_{OSL} = -\frac{dn}{dt} \equiv -\frac{dm}{dt} = np, \tag{2.8}$$

where the negative sign indicates the reduction in the concentration of electrons and holes due to recombination. The solution of equation 2.8 is

$$I_{OSL} = I_0 \exp(-pt), \tag{2.9}$$

where I_0 is the initial OSL intensity at $t = 0$ and is equal to $n_0 p$. Equation 2.9 represents an exponential decay of the OSL intensity after the stimulation light-pulse. Figure 2.2 shows an example of a CW-OSL decay curve obtained from a natural quartz sample measured at 20 ^{0}C after beta irradiation to 40 Gy.

In principle, a CW-OSL decay curve may originate from multiple traps and recombination centres. For example, the experimental decay-curve from quartz is most often described as a sum of three exponential functions,

$$I_{OSL} = I_1 \exp(-p_1 t) + I_2 \exp(-p_2 t) + I_3 \exp(-p_3 t), \tag{2.10}$$

where I_1, I_2, I_3 are scaling parameters and p_1, p_2 and p_3 are the corresponding decay constants.

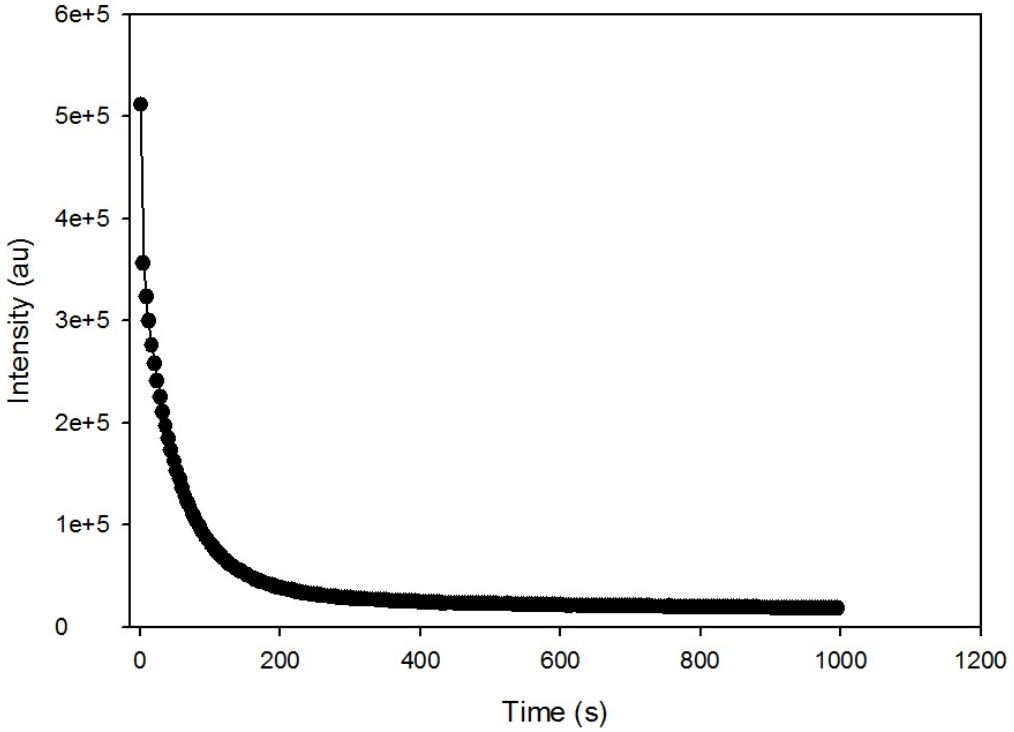

Figure 2.2: A CW-OSL decay curve obtained from quartz after beta irradiation to 40 Gy using 470 nm stimulation. The solid line is the best fit of equation 2.10.

2.1.2 Linear-modulation optically stimulated luminescence

Linear-modulation optical stimulation of luminescence (LM-OSL) is a technique whereby the stimulation power is increased linearly with respect to time and the emitted luminescence is monitored simultaneously with the stimulating light-pulse. With this method, the signal appears as a set of peaks when the luminescence intensity is plotted against time. Each peak corresponds to the optical release of charge from a particular trap. Experimentally, an LM-OSL curve may consist of more than one component resulting in a curve containing several overlapping peaks.

Figure 2.3 shows an example of an LM-OSL curve obtained from quartz after beta irradiation to 40 Gy . The measurement was made at 20^0C for 1000 seconds. The luminescence appears as a peak as shown.

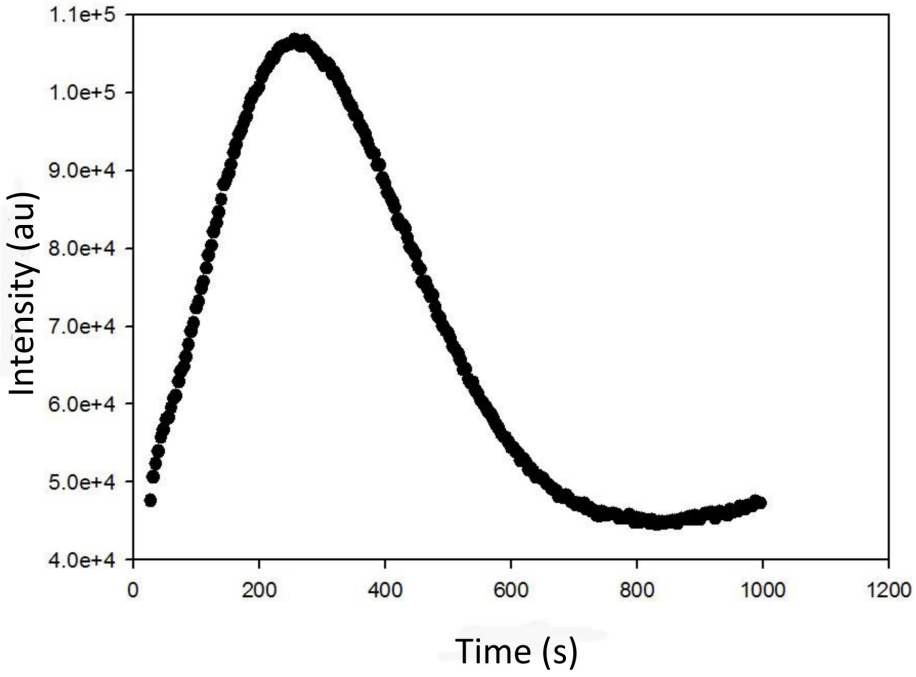

Figure 2.3: An LM-OSL curve obtained from quartz after beta irradiation to 40 Gy using 470 nm stimulation.

To describe the shape of an LM-OSL curve mathematically, we consider a one-trap and one recombination centre model as shown earlier in Figure 2.1 such that there are electrons

of concentration n in electron traps. If the stimulation intensity is linearly ramped from zero to a maximum value Φ according to

$$\Phi(t) = \gamma t, \tag{2.11}$$

where γ is the stimulation rate, then equation 2.8, rewritten below

$$-\frac{dn}{dt} = np, \tag{2.12}$$

is replaced by

$$\frac{dn}{dt} = -\sigma\gamma t n, \tag{2.13}$$

by using equation (2.4) and (2.11) in turn. Integrating equation 2.13, we find

$$n = n_0 \exp\{-\frac{\sigma\gamma}{2}t^2\}, \tag{2.14}$$

from which a solution for the LM-OSL intensity is given by

$$I_{OSL} = n_0\sigma\gamma t \exp\{-\frac{\sigma\gamma}{2}t^2\}. \tag{2.15}$$

Equation 2.15 is a Gaussian function that describes how the luminescence signal appears as a peak as a function of time. An experimental LM-OSL curve can also be described as a sum of several components. If there are k traps of type-i, equation 2.15 can be re-written as

$$I_{OSL} = \sum_{i=1}^{k} n_{0i}\sigma_i \exp\{-\frac{\gamma\sigma_i}{2}t^2\}, \tag{2.16}$$

as discussed by Whitley and McKeever [16].

2.1.3 Time-resolved optically stimulated luminescence

Time-resolved optically stimulated luminescence (TR-OSL) is the third mode used to optically stimulate luminescence. TR-OSL involves the use of pulsed light to stimulate luminescence from an irradiated material. Time-resolved optically stimulated luminescence separates in time the stimulation and emission of the luminescence [14].

A time-resolved spectrum has two portions; the signal during the stimulation light-pulse and the luminescence after the light-pulse. The fall of the emitted luminescence after the light-pulse is characterized by a decay time called the luminescence lifetime τ. The luminescence lifetime is the delay between the stimulation and emission of luminescence.

Figure 2.4 shows an example of a TR-OSL spectrum from a sample of quartz following beta irradiation to 120 Gy before pulsed stimulation. As shown in Figure 2.4, the TR-OSL spectrum consists of two portions, the increase in the signal during the pulse and the decrease in luminescence after the pulse. Since this project focusses on the design of a pulsing system for measurement of TR-OSL, the next chapter discusses TR-OSL in detail.

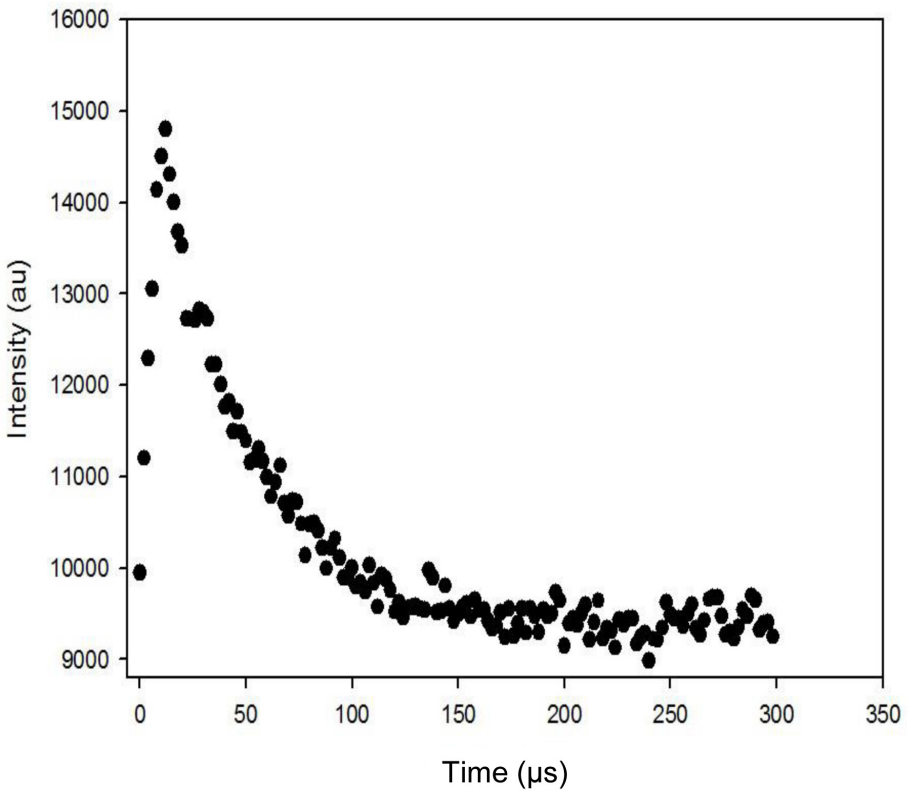

Figure 2.4: A TR-OSL spectrum from a sample of natural quartz. The sample was irradiated to 120 Gy before pulsed stimulation using 470 nm LEDs.

Chapter 3

Time-resolved optically stimulated luminescence

3.1 Introduction

Time-resolved optically stimulated luminescence (TR-OSL) is measured when an irradiated sample is pulsed-stimulated at a selected pulse-width. This technique has been used to study mechanisms of luminescence in quartz and feldspar [17, 18, 19] and α-Al_2O_3:C [20], materials of interest in dosimetry.

TR-OSL measurements are carried-out using a brief light-pulse to stimulate luminescence. A detector, for example, a photomultiplier tube detects the emitted luminescence. During stimulation, the luminescence increases over a background of photomultiplier noise and scattered stimulating light. After the light-pulse, the emitted luminescence is measured over photomultiplier noise. The detected luminescence from several scans are summed giving rise to a time-resolved luminescence spectrum.

The TR-OSL spectrum is generated by timing the duration between a START and a STOP signal. A multichannel scaler produces a START signal that triggers a pulsing sys-

tem to turn ON LEDs for stimulation. The first luminescence-photon signal detected from a particular sample under stimulation provides a valid STOP signal. The multichannel scaler then records the luminescence-photon counting rate until a STOP signal arrives.

A time-resolved luminescence spectrum consists of two portions, the signal during stimulation and the signal after stimulation. The luminescence either during or following the light-pulse can be analysed for lifetimes [13]. The luminescence lifetime, τ, is the delay between stimulation and emission of luminescence [13]. There are three principal mechanisms that are thought to influence this delay: the time to evict an electron from a trap, electron transit-time between trap and recombination centre through the conduction band and, the lifetime of the excited state at the recombination centre [15]. Of these, the relaxation time at the recombination centre is dominant [15].

Chithambo [15] studied the luminescence lifetime during and after the stimulation pulse and noted that the luminescence lifetime evaluated from either portion of a time-resolved spectrum should be similar since recombination processes during or after stimulation are the same. Chithambo [15] reported luminescence lifetimes of 31.3 $\pm$ 3.4 μs and 31.6 $\pm$ 0.8 μs during stimulation and after stimulation respectively from an irradiated sample of quartz pulsed stimulated at 470 nm. Lifetimes enable the study of recombination in a material thereby providing important information on the underlying mechanisms of luminescence [14, 21, 15].

3.2 Models of time-resolved optically stimulated luminescence

Models of TR-OSL are aimed at describing mechanisms involved in the emission of time-resolved luminescence as well as methods for analysis of TR-OSL spectra. Three different models have been described by Chithambo [14, 15]; Pagonis et al. [21, 22] and, Yukihara

and McKeever [5] respectively. The models are now discussed.

3.2.1 The model of Chithambo [14, 15]

Chithambo [14, 15] developed a phenomenological model for TR-OSL where both portions of the TR-OSL spectrum are analytically described. The model is based on one recombination centre and, one electron trap with an initial concentration A with a probability of stimulation per unit time s, and a decay constant λ representing the probability per unit time that a stimulated electron will produce luminescence. N is the number of stimulated electrons.

During stimulation, the rate of change of the number of stimulated electrons N is given by

$$\frac{dN}{dt} = sA - \lambda N, \tag{3.1}$$

from which the time-dependence of the number of stimulated electrons $N(t)$ is

$$N(t) = \frac{sA}{\lambda}[1 - \exp(-\lambda t)]. \tag{3.2}$$

Equation 3.2 is a saturating exponential function since $N(t)$ increases during pulsed stimulation to a particular maximum. Since the production of luminescence, L, following radiative decay of stimulated electrons is expressed as

$$dL(t) = \lambda N(t)dt, \tag{3.3}$$

the rate of luminescence emission during pulsing is given as

$$l_1(t) = sA[1 - \exp(-\lambda t)]. \tag{3.4}$$

Equation 3.4 describes a saturating exponential and shows that during pulsed optical stimulation, the rate of trap emptying and hence luminescence recombination increases approximately towards some limiting maximum [14].

After the stimulation light pulse of width t_1 is turned off, the luminescence decays away as

$$l_2(t) = sA\exp(\lambda t)[\exp(\lambda t_1) - 1)]. \tag{3.5}$$

Equation 3.5 is an exponential decay function.

Since the luminescence after the stimulation pulse is measured in addition to the photomultiplier noise, the portion of each TR-OSL spectrum after the pulse obtained from experiment is fitted to an exponential function of the form

$$I(t) = \sum_i A_i \exp(-\lambda_i t) + B, \tag{3.6}$$

where λ_i is the decay constant of the ith component, A_i a scaling parameter for the ith component, t the stimulation time and B is a constant added to account for the background. The exponential function in equation 3.6 shows the decrease of luminescence after the stimulation pulse.

3.2.2 Kinetic model of Pagonis et al. [21, 23]

Pagonis et al. [21, 23] developed a kinetic model for TR-OSL in quartz. Figure 3.1 is a schematic diagram of the kinetic model of Pagonis et al. [21, 23] in quartz. The model consists of an electron trap (level 1), and three energy levels within the recombination centre with electronic transitions taking place from the trap through the conduction band to the recombination centre. From the electron trap, electrons are stimulated by optical stimulation into the conduction band (CB) with some of these electrons being retrapped with a probability A_n. Transition 3 indicates an electronic transition from the CB into the

excited state below the CB, with probability A_{CB}. The direct radiative transition from excited level into the ground electronic state of the recombination centre, with probability A_R is shown in transition 5. Transition 4 corresponds to a competing thermal assisted process represented by a Boltzmann constant of the form $A_{NR}\exp(-W/kT)$, where W denotes the activation energy for this process and A_{NR} represents the non-radiative transition probability. A non-radiative transition into the ground electronic state is shown in transition 6.

In Figure 3.1, n_1 is the concentration of electrons in the electron trap, N_1 the total concentration of the electron traps (cm^{-3}), n_2 the concentration of electrons in the excited state of the recombination centre and N_2 total concentration of recombination centres (cm^{-3})

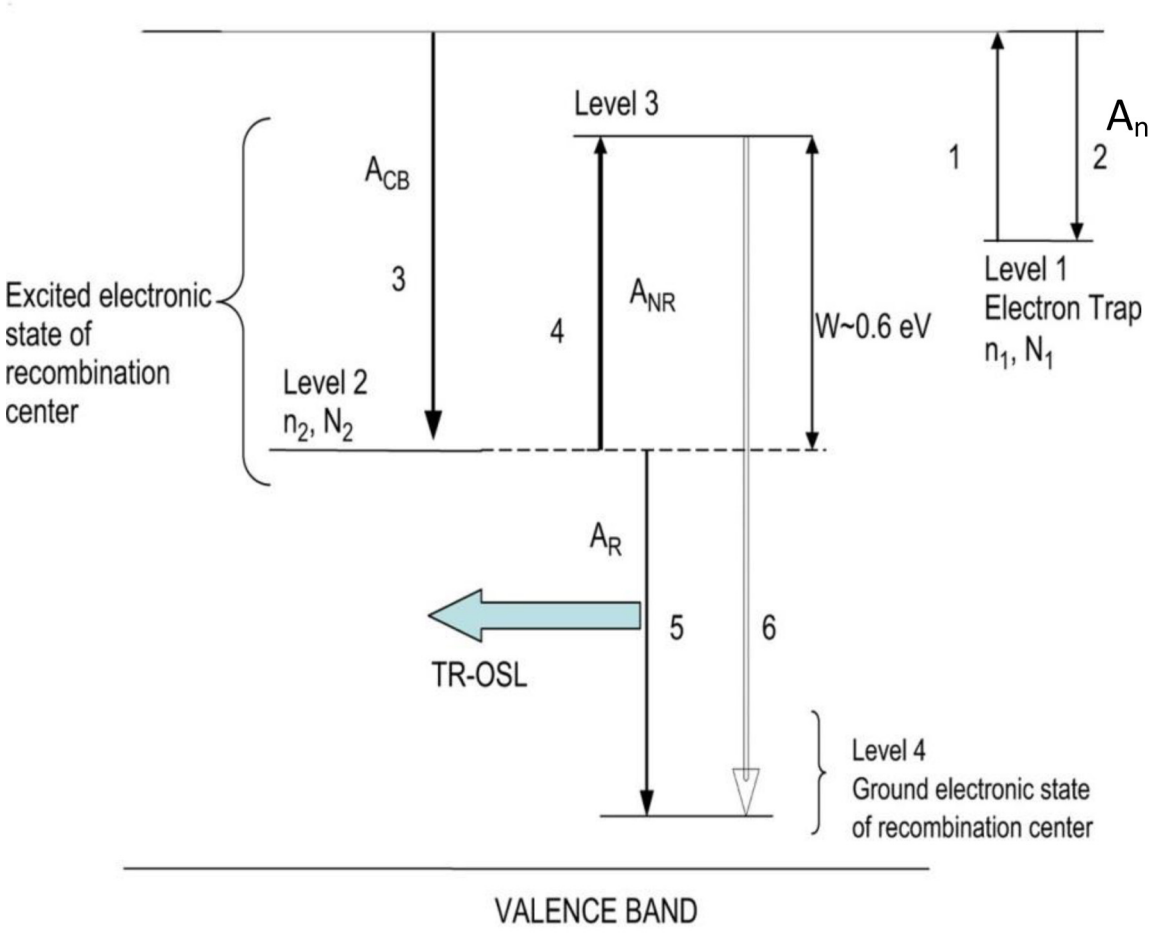

Figure 3.1: A schematic diagram of the kinetic model for quartz which contains an electron trap (level1), two excited states within the radiative recombination centre (levels 2 and 3). Level 4 is the ground electronic state of recombination centre [21, 23].

During the stimulation light-pulse, the concentration of electrons n_c in the CB is given by

$$n_c(t) = \frac{n_1(0)p}{A_n(N_1 - n_1(0)) + A_{CB}N_2}(1 - e^{-[A_n(N_1 - n_1(0) + A_{CB}N_2]t}), \tag{3.7}$$

where $n_1(0)$ is the concentration of electrons in the electron trap at the beginning of the stimulation and p the probability of optical excitation of electron from the electron trap (in units of s^{-1}). Equation 3.7 is a saturating exponential function. After the stimulation light-pulse of duration t_0 is turned off, the time-dependence of concentration of electrons

$n_c(t)$ is given by

$$n_c(t) = n_c(t_0) \exp^{-[A_n(N_1 - n_1(0)) + A_{CB}N_2](t-t_0)}, \tag{3.8}$$

where $n_c(t_0)$ is the concentration of electrons at the end of the TR-OSL pulse. Equation 3.8 is an exponential decay function since $n_c(t)$ starts to decrease after the stimulation pulse. The time-dependence of concentration of electrons in the excited state of the recombination centre $n_2(t)$ during stimulation is given by

$$\frac{dn_2}{dt} = \frac{n_1(0)pA_{CB}N_2}{A_n(N - n_1(0)) + A_{CB}N_2} - n_2(A_R + A_{NR}\exp(-W/kT)). \tag{3.9}$$

where k is Boltzmann constant. Equation 3.9 describes the time-dependence of concentration of electrons in the excited state of the recombination centre involving thermal assisted process at the recombination centre.

After the stimulation pulse, $n_2(t)$ is given by

$$n_2(t) = n_2(t_0) \exp^{-[A_R + A_{NR}\exp(-W/KT)](t-t_0)}. \tag{3.10}$$

Equation 3.10 is an exponential decay function.

The time-dependence of the luminescence intensity $l(t)$ during the stimulation pulse is given by

$$l(t) = A_R \frac{f}{A_R + A_{NR}\exp(-W/KT)}(1 - e^{-[A_R + A_{NR}\exp(-W/KT)]t}), \tag{3.11}$$

where $f = \frac{n_1(0)PA_{CB}N_2}{A_N(N_1 - n_1(0) + A_{CB}N_2}$ is a constant. Equation 3.11 is a saturating exponential function. The time-dependence of the luminescence intensity after the end of the stimulation pulse is given by

$$l(t) = A_R n_2(t_0) e^{-[A_R + A_{NR}\exp(-W/KT)](t - t_(0)}. \tag{3.12}$$

Equation 3.12 is an exponential decay function.

The luminescence lifetime τ of the recombination centre is given by

$$\tau = \frac{1/A_R}{1 + \frac{A_{NR}}{A_R}\exp(-W/KT)} = \frac{\tau_o}{1 + C\exp(-W/KT)} \tag{3.13}$$

Equation 3.13 describes the effect of temperature on luminescence lifetimes due to increased probability of non-radiative transitions at high temperature, a phenomenon known as thermal quenching.

3.2.3 Models of Yukihara and Mckeever [5]

Yukihara and McKeever [5] derived an expression for TR-OSL intensity during and after the stimulation pulse. They described the time-dependence of the concentration of the recombination centres in the excited state $m^*(t)$ during stimulation pulse as

$$\frac{dm^*(t)}{dt} = -\frac{m^*(t)}{\tau} + n_0 p e^{-pt}, \tag{3.14}$$

where τ represents the luminescence lifetime, n_0 is the initial concentration of trapped electrons and p the stimulation rate of the trapping centres. Equation 3.14 states that the concentration of excited recombination centres m^* decreases due to relaxation which occurs with a probability equal to τ^{-1} and, increases at the same rate as the concentration of trapped electrons n decreases due to recombination.

In the model of Yukihara and McKeever [5], the luminescence intensity $l(t)$ during the stimulation light pulse is given by

$$l_1(t) = m_0^* e^{-t/\tau} + \frac{n_0 p}{-p + \tau^{-1}}(e^{-pt} - e^{-t/\tau}), \tag{3.15}$$

where m_0^* is the initial concentrations of the excited luminescence centres at the start of each stimulation pulse respectively. Equation 3.15 shows that the luminescence increases

during stimulation. The luminescence intensity after the stimulation light pulse is given by

$$l_2(t) = m^*(\Delta t)e^{-t/\tau}/\tau, \tag{3.16}$$

where $m^*(\Delta t)$ represents the concentration of excited centres at the end of a stimulation pulse of duration Δt. Equation 3.16 shows the exponential decay of the luminescence signal after the stimulation pulse.

3.2.4 Dynamic throughput

The dynamic throughput f was introduced and defined by Chithambo [14] as the ratio of the luminescence L_2 emitted after the pulse to the total integrated luminescence L_T and is given by

$$f = \frac{L_2}{L_T} = \frac{1}{\lambda t_1}[1 - \exp(-\lambda t_1], \tag{3.17}$$

where λ is the decay constant and t_1 is the time after the stimulation light-pulse. The luminescence lifetime $\tau = \frac{1}{\lambda}$. Equation 3.17 shows that the amount of luminescence detected increases as the pulse-width becomes a small fraction of the luminescence lifetime for a given dynamic range [14]. In other words, Equation 3.17 shows that the amount of luminescence recorded under pulsed optical stimulation should increase significantly when the stimulating pulse-width is decreased to a small fraction of the luminescence lifetime [15].

3.3 Inter-comparison of models

This section briefly compares models of TR-OSL presented earlier. TR-OSL consists of two portions; the luminescence signal during and, after the stimulation light-pulse.

The rate of change of the number of stimulated electrons N during stimulation was described by Chithambo [14, 15] as

$$\frac{dN}{dt} = sA - \lambda N. \tag{3.18}$$

In comparison, Pagonis et al. [21, 23] described the rate of change of the concentration of electrons n_2 in the excited state of the recombination centre as

$$\frac{dn_2}{dt} = \frac{n_1(0)PA_{CB}N_2}{A_n(N - n_1(0)) + A_{CB}N_2} - n_2(A_R + A_{NR}\exp(-W/KT)). \tag{3.19}$$

On the other hand, Yukihara and McKeever [5] did not use the change in the concentration of electrons but that of the recombination centres. The time-dependence of the concentration of excited recombination centres $m^*(t)$ described by Yukihara and McKeever [5] is given by

$$\frac{dm^*(t)}{dt} = -\frac{m^*(t)}{\tau} + n_0 p e^{-pt}. \tag{3.20}$$

If we assume small retrapping probability $A_n(N_1 - n_1(0)) \ll A_{CB}N_2$ [21] at the recombination centre, Equation 3.19 becomes

$$\frac{dn_2}{dt} = n_1(0)p - n_2(A_R + A_{NR}\exp(-W/KT)). \tag{3.21}$$

The constants A and s in Equation 3.18 can be identified with $n_1(0)$, p in Equation 3.21, respectively. The decay constant λ is identified with the luminescence probability per unit time, $A_R + A_{NR}\exp(-W/KT)$.

The rate of luminescence emission during stimulation $l(t)$ described by Chithambo [14, 15] is given by

$$l_1(t) = sA[1 - \exp(-\lambda t)], \tag{3.22}$$

whereas the luminescence emitted during stimulation is described by Pagonis et al. [21, 23] as

$$l(t) = A_R \frac{f}{A_R + A_{NR}\exp(-W/KT)}(1 - e^{-[A_R + A_{NR}\exp(-W/KT)]t}). \tag{3.23}$$

Yukihara and McKeever [5] described the luminescence emitted during stimulation as

$$l_1(t) = m_0^* e^{-t/\tau} + \frac{n_0 p}{-p + \tau^{-1}}(e^{-pt} - e^{-t/\tau}). \tag{3.24}$$

In all the models, the rate of luminescence emitted increases exponentially during the stimulation light-pulse.

The rate of luminescence emitted after the stimulation light-pulse is given by Chithambo [14, 15] as

$$I(t) = \sum_i A_i \exp(-\lambda_i t) + B. \tag{3.25}$$

Pagonis et al. [21, 23] described the rate of luminescence emitted at the recombination centre after the light-pulse as

$$l(t) = A_R n_2(t_0) e^{-[A_R + A_{NR}\exp(-W/KT)](t - t_0)}, \tag{3.26}$$

whereas Yukihara and McKeever [5] described the rate of luminescence emitted as

$$l_2(t) = m^*(\Delta t) e^{-t/\tau}/\tau. \tag{3.27}$$

The models of Chithambo [14, 15], Pagonis et al. [21, 23] and Yukihara and McKeever [5] yield similar results for both portions of the TR-OSL spectrum even though they were derived using different approaches. For example, the model of Chithambo [14, 15] was derived from empirical considerations while that of Pagonis et al. [21, 23] model was derived from modelling of TR-OSL experiment. When modelling TR-OSL, the kinetic parameters $n_1(0), p, A_R, A_{NR}, n_2$, and N take on specific values. In the case of the model

of Chithambo [14, 15] these kinetic parameters are assumed to be constant. In the model of Yukihara and McKeever [5] these kinetic parameters take on specific values.

3.4 Applications

There are many applications of TR-OSL reported in the literature. For example, TR-OSL has been used extensively to study luminescence mechanisms in quartz [17, 24, 25] and in α-Al_3O_3:C [11, 26, 27], materials of importance in dosimetry. In this study, two applications of TR-OSL are briefly discussed.

Chithambo et al. [28] used TR-OSL to study the effect of geological provenance on luminescence lifetimes of low sensitivity natural quartz from crystalline rocks. Samples of natural quartz separated from plutonic, metamorphic, hydrothermal and volcanic rocks were used for the study. In all the samples studied by Chithambo et al. [28], two different values of luminescence lifetimes were obtained. All the samples showed short luminescence lifetime less than 5 μs. The value of the second lifetime being the principal lifetime changes considerably in all samples. In metamorphic quartz formed at temperatures between 450 - 550 ^{0}C, the value of the principal lifetime was 86 μs. In plutonic quartz formed at temperatures between 550 - 700 ^{0}C, the value of the principal lifetime was 18 μs. In hydrothermal quartz formed at a temperature of about 400 ^{0}C, the value of the principal lifetime was 100 μs. Chithambo et al. [28] attributed this change in luminescence lifetimes to the thermal provenance of the quartz arguing that the annealing influenced the size of the observed lifetime. Chithambo et al. [28] further explained their results with a model consisting of three luminescence centers with the dominant lifetime linked to preferential recombination at one center depending on the thermal history of the sample and hence the hole concentration of the center [28].

Pagonis et al. [29] used TR-OSL and radioluminescence to study the correlation between the change of luminescence lifetimes and emission band with annealing temperature in sedimentary quartz. Pagonis et al. [29] developed a model to explain the change of luminescence lifetimes with annealing and measurement temperature in sedimentary quartz. Luminescence lifetimes in quartz of sedimentary origin is independent of annealing temperature below 500 ^{0}C but decreases with annealing and measurement temperature above 600 ^{0}C. Pagonis et al. [29] used radioluminescence to study the emission band at the recombination centre using the same annealed sedimentary quartz. Indeed, the emission band decreases with an increase in annealing temperature. Annealing at 500 ^{0}C induced a strong emission band at $\sim$ 3.42 eV (360 nm) which decreased significantly to $\sim$ 3.73 eV (330 nm) for annealing temperatures above 600 ^{0}C. The authors explained the observed change of lifetime using an extended model that included two luminescence centres L_H and L_L as well as a hole reservoir. The model involves localized electronic transitions between energy states within two luminescence centers. Figure 3.2 shows the schematic representation of the model used by Pagonis et al. [29] to explain the luminescence lifetimes in annealed quartz. The figure consists of two luminescence centres, each with its own distinct luminescence lifetimes τ_L and τ_H, an electron trap and a ground state of the radiative centre. The behaviour of the emission band at $\sim$ 3.73 eV was found to be qualitatively correlated with the hypothesized behaviour of the concentration of holes N_L of the recombination center L_L in the model.

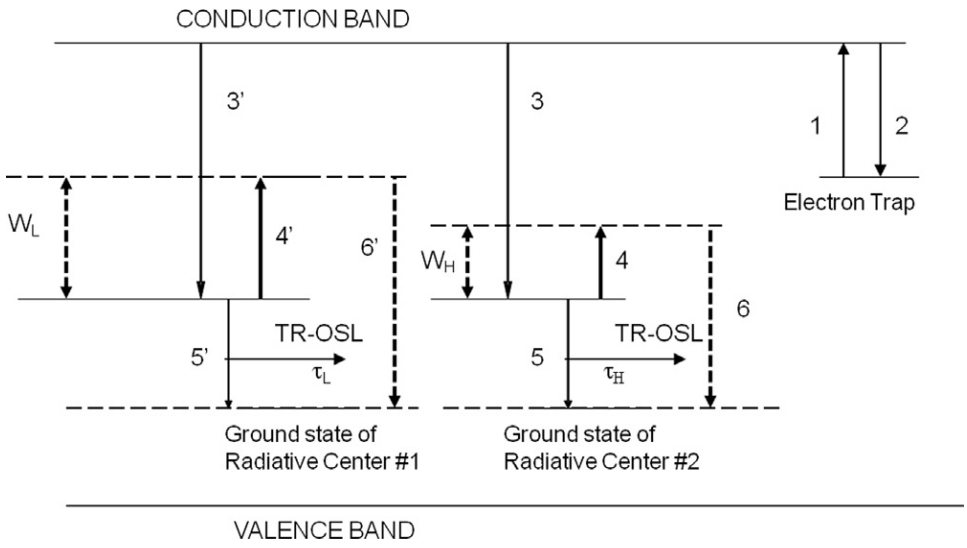

Figure 3.2: The model used by Pagonis et al. [29] to explain luminescence lifetimes in annealed quartz. The model consists of two luminescence centres L_H and L_L, each with its own distinct luminescence lifetime τ_L or τ_H.

Chapter 4

Design of the new pulsing system

4.1 Introduction

This chapter describes the new pulsing system developed in this project. The system consists of pulsing circuitry capable of operating a stimulating light source.

4.2 Design considerations

Figure 4.1 shows a schematic diagram of the pulsing system. Figure 4.1(a) shows the schematic arrangement for detection and measurement of time-resolved luminescence spectra. Figure 1(b) is a schematic diagram of the circuitry used for pulsing. The detecting system shown in Figure 4.1(a) was reported previously by Galloway[30] and Chithambo [9]. The original design was reported by Chithambo and Galloway [13] and discussed by Chithambo [31]. The pulsing circuit shown in Figure 4.1(b) is new and is discussed in detail in this chapter.

Luminescence is stimulated by a set of 16 LEDs arranged in a dural holder. A Schott GG-420 long-pass filter was placed in front of each LED to prevent scattered stimulation light from reaching the photomultiplier tube. A Schott BG39 transmission filter, with a

transmission peak at 340 nm was placed in front of the photomultiplier tube to transmit the emitted luminescence to the photomultiplier tube.

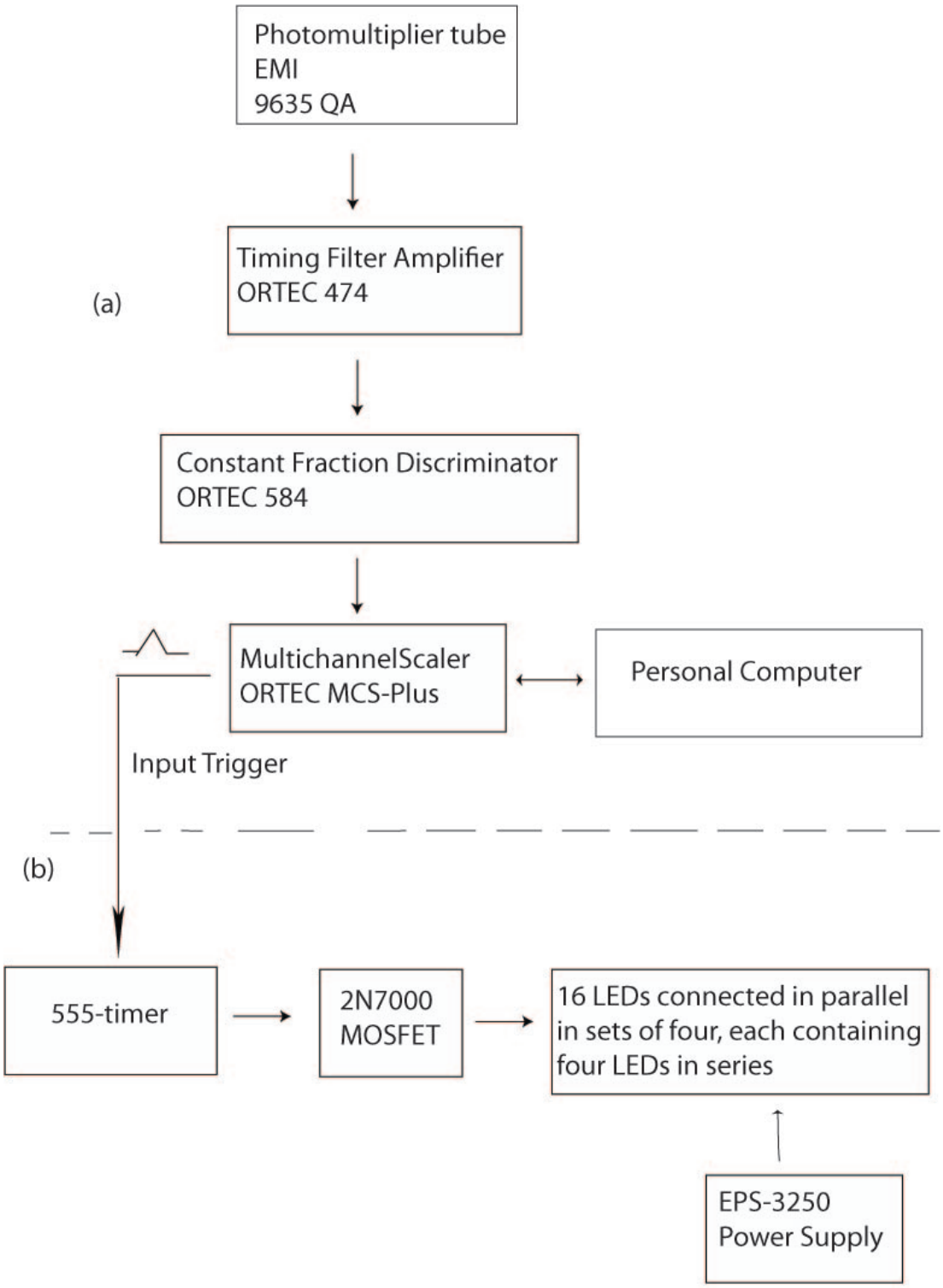

Figure 4.1: The pulsing system showing the arrangement for detecting and recording time-resolved luminescence spectra (a) and the pulsing circuitry used to pulse the light-emitting-diodes (b).

As shown in Figure 4.1, the emitted luminescence is detected by a photomultiplier tube (EMI 9635QA) and the signal fed into the combination of a timing filter amplifier (Ortec 474) and a constant-fraction discriminator (Ortec 584).

The ORTEC Model 474 timing filter amplifier is designed to shape pulses and optimize the signal-to-noise ratio for timing measurements [32]. These pulses from the photomultiplier tube are then furnished to an Ortec 584 constant-fraction discriminator where they are counted.

The multichannel scaler (Ortec MCS-plus^{TM}) simultaneously triggers the pulsing circuitry and records the counting rate of events as a function of time as shown in Figure 4.1. In this context, an event is the detection of a photon. Once a scan is started, the multichannel scaler begins counting the luminescence photons emitted at a preset dwell-time in the first channel of its memory. The MCS then moves to the next channel of its memory to do same until all channels are covered. A display of the content of memory shows the counting rate of recorded data as a function of time.

4.2.1 Pulsing circuitry

The pulsing circuit produces pulses of various duration using a 555-timer that was triggered externally by the multichannel scaler. The output pulse from the 555-timer is fed into a 2N7000 MOSFET transistor. The 2N7000 MOSFET was used to increase the pulse-current obtained from the 555-timer circuitry.

4.2.1.1 Operation of the pulsing circuitry

Figure 4.2 shows the circuitry of the pulsing system. In the circuitry, a monostable multivibrator based on the NE555N timer integrated circuit was used to produce pulses of various duration. Figure 4.2(a) shows the circuitry of an NE555N timer operated as a monostable multivibrator whereas Figure 4.2(b) shows the LED drive circuitry.

In Figure 4.2(a), the voltage of pin 2 is held above the trigger point (i.e $> \frac{1}{3}$ of input voltage V_{CC}) by the R1 pull-up resistor of value 10 kΩ until a voltage pulse to trigger a timing cycle is applied from the multichannel scaler.

In quiescent condition, pin 7 of the NE555N timer is conducting to ground and represents a short circuit across the timing capacitor C1. The level of the output (pin 3) is always low at this point. To obtain an output transition from LOW to HIGH, an external input trigger-pulse of amplitude greater than $+\frac{2}{3}$ V_{CC} is applied to pin 2 of the NE555N timer from the multichannel scaler. As a result, the voltage of pin 2 drops below $\frac{1}{3}V_{CC}$ and forces the output of pin 3 to go HIGH to a value slightly above V_{CC}. Since pin 7 is cut-off, capacitor C1 begins to charge exponentially and the voltage across it also increases exponentially from zero until it reaches $\frac{2}{3}V_{CC}$ through the resistor R2 with a time-constant equal to the product R2·C1. When the voltage of capacitor C1 becomes slightly greater than its threshold of $+\frac{2}{3}$ V_{CC}, pin 6 goes HIGH, thereby causing capacitor C1 to discharge. Thus, the output of pin 3 of the timer goes LOW that is transits back from HIGH to LOW. The capacitor C1 discharges rapidly, and the output is held in its LOW state (V_{out} = LOW) until another trigger pulse is applied to pin 2 from the multichannel scaler. It should be noted that pin 4 is connected to V_{CC} to prevent accidental reset while pin 5 is held to ground through a 0.01 μF capacitor C2 to help reduce background noise.

The output pulse-width of the pulsing circuitry is defined by the external resistor (R2) and capacitor (C1). The pulse-width t_w is given approximately by

$$t_w = 1.1(R1)(C1). \tag{4.1}$$

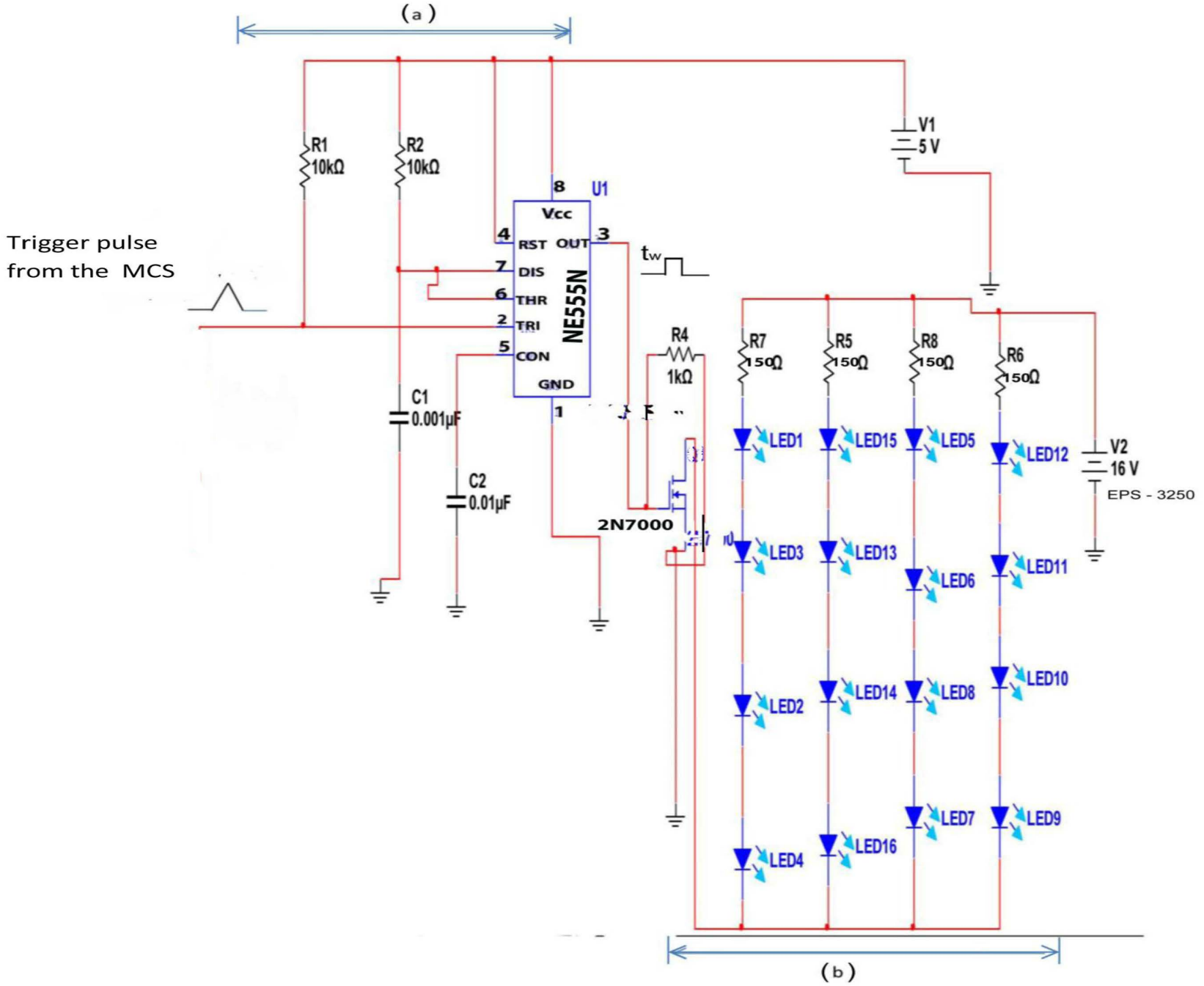

Figure 4.2: A circuitry showing an NE555N timer operated as a monostable multivibrator when triggered with a trigger pulse from a multichannel scaler (a) and the LED drive circuitry showing the connection of the sixteen blue light-emitting-diodes to an 2N7000 MOSFET (b).

4.2.2 Drive circuitry for LEDs

Figure 4.2(b) shows the circuit used to operate the light-emitting-diodes. The output pulse obtained from the pulsing circuitry is fed into the gate pin of an 2N7000 MOSFET which then supplies sufficient pulse-current to the LEDs. The source pin of the 2N7000 is earthed while the drain pin is connected to the LEDs. The 2N7000 MOSFET is used as a switch to increase the pulse-current obtained from the NE555N timer circuitry. The 2N7000 can switch a maximum pulse-current of 500 mA, with a maximum ON-resistance of 5 ohm at 4.5 V Vgs. Sixteen LEDs are connected in parallel in sets of four, each set containing four LEDs in series. Each LED is driven at 90 mA pulse-current with a possible maximum of 110 mA per LED. The intensity of the LED light can be controlled and regulated by an integrated adjustable power supply (shown as EPS-3250 in Figure 4.2) of constant current. To pulse the LEDS, the pulsing circuitry is triggered with a trigger pulse from a multichannel scaler.

4.2.3 Pulse-width control unit

Figure 4.3 shows the circuit used to vary the pulse-width. A potentiometer with resistance values ranging from 0 to 500 kΩ connected to a 0.1 μF fixed capacitor was used to obtain pulses of various width from the 555 timer. One of the two end-pins of the potentiometer is connected to a 5 V supply voltage whereas the center-pin is connected to one of the terminals of the fixed capacitor (the other terminal of the capacitor is connected to earth). This set-up was used to obtain various pulses of width between 4.7 μs to 489 ms. The output pulse obtained with the system becomes distorted when approaching the nanosecond range. Thus the output pulse-width is stable only from microseconds upwards.

Figure 4.4 shows examples of pulses of different width obtained from the pulsing system. These output pulses were measured with a Tektronix oscilloscope.

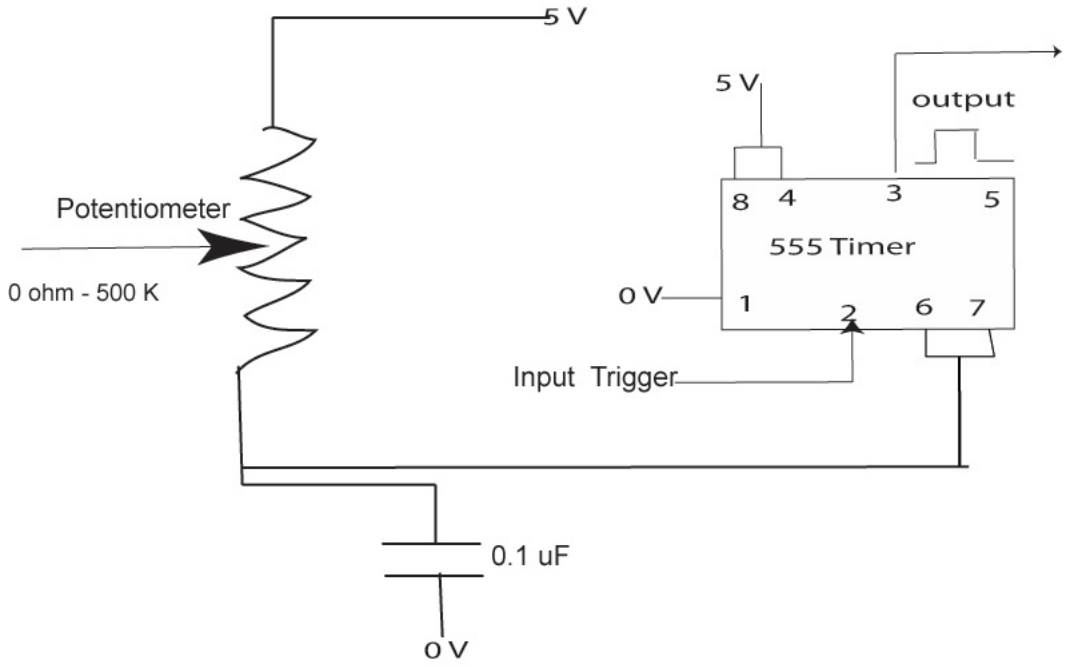

Figure 4.3: A circuit showing the connection of the 555 timer to a potentiometer and a 0.1 μF fixed capacitor.

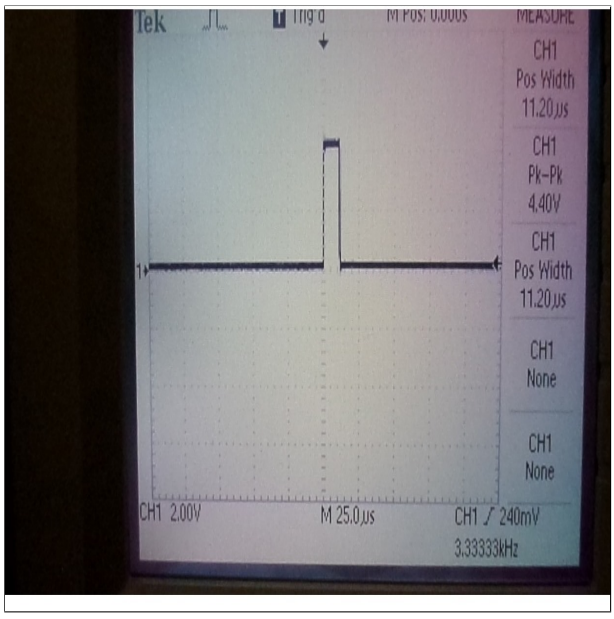

(a)

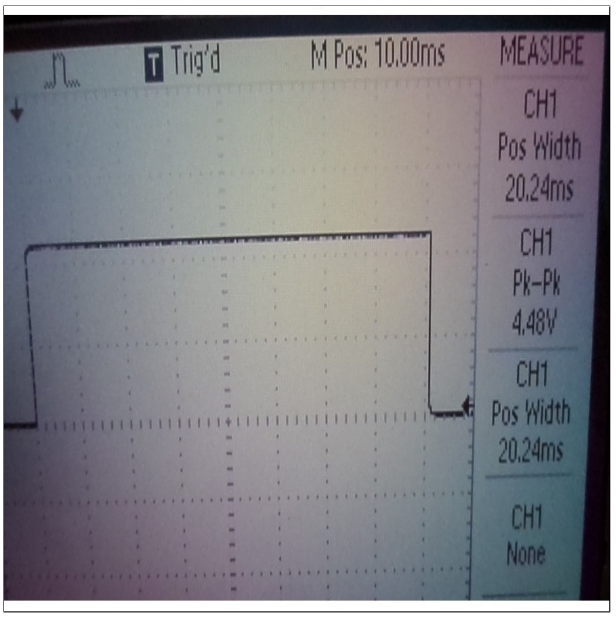

(b)

Figure 4.4: Examples of two pulses of different widths obtained automatically from the pulsing system. Part (a) shows an 11.2 μs pulse whereas part (b) shows a 24.24 ms pulse.

4.2.4 Control of the intensity of light-emitting-diodes

The intensity of the stimulation light is controlled and regulated by an integrated adjustable power supply (EPS-3250) of constant current. The power supply is capable of adjustable voltage from 0 to 20 V. Since the voltage from the EPS-3250 across the LEDs is forward-biased, the pulse-current from the 2N7000 flows through the LEDs in forward direction as shown in Figure 4.1(b). The intensity of the LEDs increases when the supply voltage is increased.

4.3 Spectral features of stimulating light

The study of the emission spectra of light-emitting-diodes for stimulating luminescence is important because of the need to separate the luminescence from scattered stimulating light by the use of optical filters [33]. Spectral measurements of blue light-emitting-diodes operated at different pulse-currents were done. The spectral measurements were done using a Daedalon E0-85 spectrophotometer. The spectrophotometer is based on a 700 lines/mm holographic grating whose first-order spectrum focuses onto a high resolution linear CCD detector. The spectrophotometer has a wavelength range between 400 and 800 nm. In addition, spectra of a total of six different light-emitting-diodes were measured at a nominal current of 20 mA. All spectral measurements were compared with specifications from the LED manufacturers.

4.3.1 Calibration of spectrophotometer

In order to measure emission spectra of the light-emitting-diodes, calibration of the spectrophotometer was necessary. An experiment was conducted to calibrate the spectrophotometer. The spectrophotometer was calibrated using a mercury lamp as a reference

source. Spectrum of this lamp was first obtained via measurement using the spectrophotometer software. As the spectrum from the lamp was displayed, the spectrophotometer was then calibrated using the calibration button in the software.

4.3.2 Measurement of LED spectra

Here, we present the spectral properties of six different light-emitting-diodes measured at a nominal current of 20 mA. Figure 4.5 shows the emission spectra of six different LEDs. The Nichia NSPB500AS blue LED showed an emission peak-wavelength of 470.0 ± 0.1 nm with a full width at half maximum (FWHM) of 25 nm. The value was the average of five measurements. The 470.0 ± 0.1 nm peak wavelength obtained is consistent with the manufacturer's specification which is 470 nm.

The peak-wavelength for each of the remaining five other LEDs is shown in Table 4.1. The NSPG500DS, L-53MBC, HLMP-C515, L-7113EC and L-715135 LEDs showed an emission peak wavelengths of 524.5 ± 0.1, 429.8 ± 0.1, 570.1 ± 0.2, 628.0 ± 0.2 and 659.8 ± 0.2 nm respectively and FHWM of 40, 81, 35, 40 and 20 nm respectively. The peak-wavelength obtained for these five LEDs are also consistent with their manufacturer's specifications.

Figure 4.6 shows a plot of the measured peak-wavelength against the specified peak-wavelength. The measured peak-wavelength is consistent with specified peak-wavelength. Thus, the spectral measurements on the six different light-emitting-diodes are in good agreement with the manufacturer's specifications.

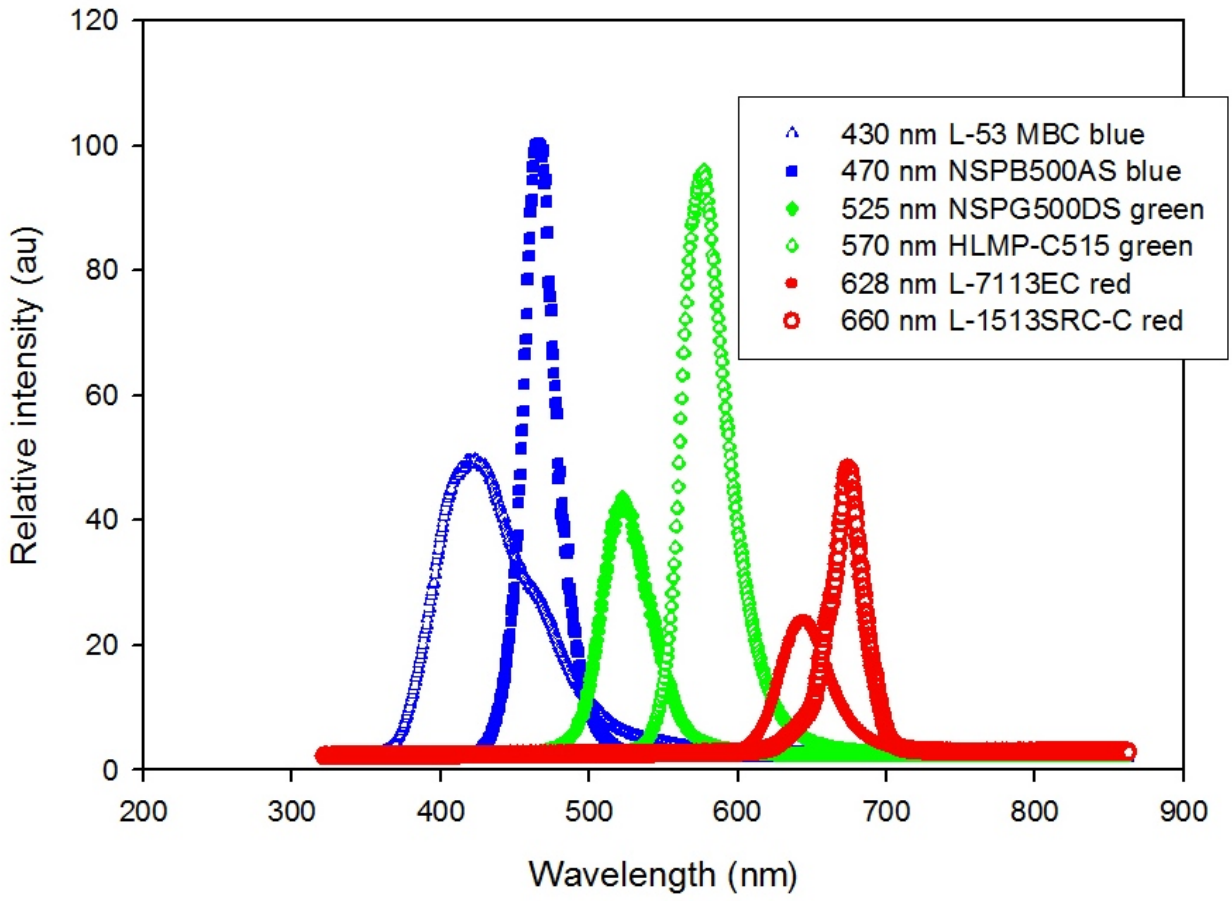

Figure 4.5: Results from spectral measurements on six different LEDs measured at a nominal current of 20 mA. Full width at half maximum are given in the text. These measurements were partly for use in calibrating the Daedalon EO-85 spectrophotometer.

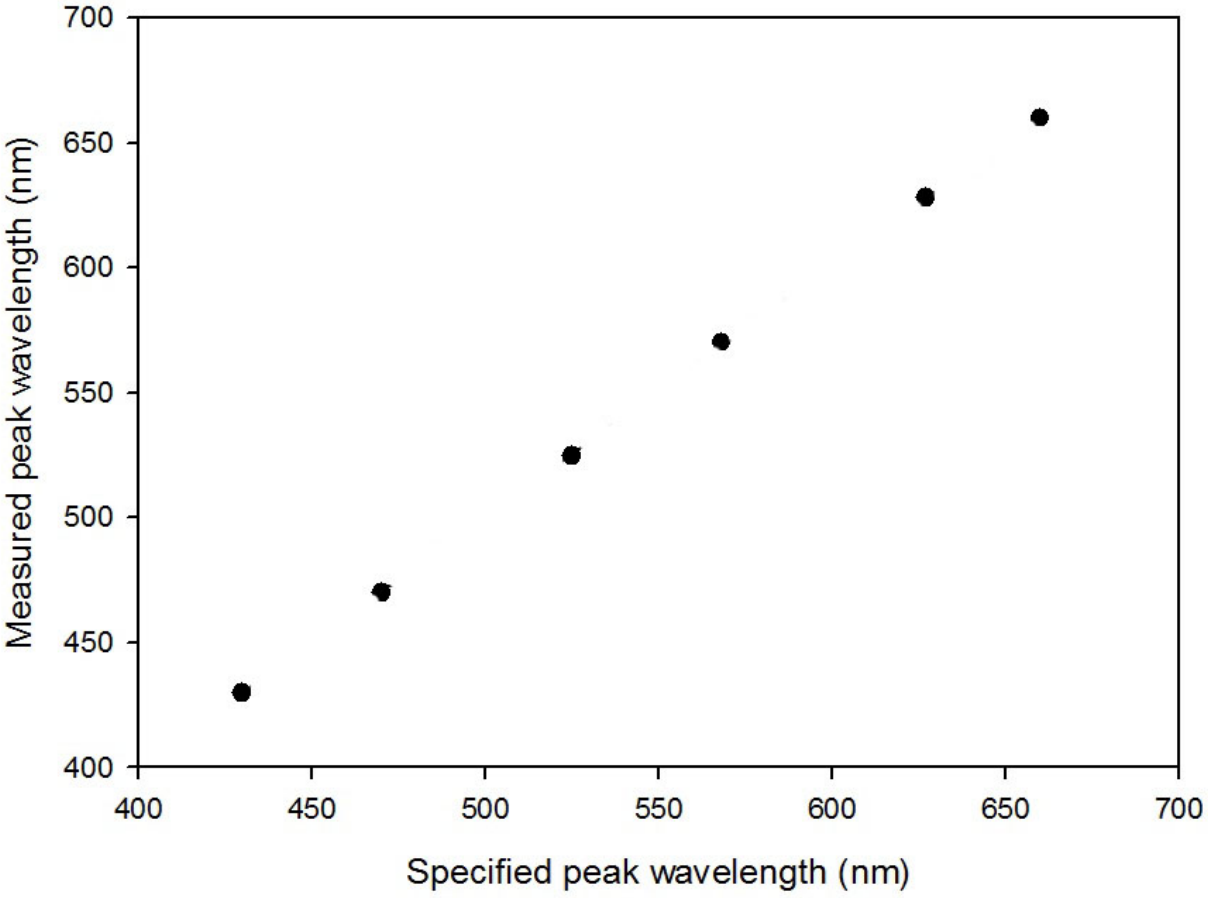

Figure 4.6: A plot of measured peak-wavelength of six different light-emitting-diodes as a function of peak-wavelength as specified by the manufacturers.

Table 4.1: Spectral properties of six different LEDs measured at 20 mA nominal current. Spectral results are compared with the manufacturer's specifications.

LED type	LED Colour	Specified Peak Wavelength (nm)	Measured Peak Wavelength (nm)	Specified FWHM (nm)	Measured FWHM (nm)
NSPB500AS*	Blue	470	470.0 ± 0.1	...	25
L-53MBC**	Blue	430	429.8 ± 0.2	...	81
NSPG500DS*	Green	525	524.5 ± 0.1	...	40
HLMP-C515***	Green	568	570.1 ± 0.2	....	35
L-7113EC***	Red	627	628.0 ± 0.2	45	40
L-1513SRC-C***	Red	660	659.8 ± 0.2	20	20

*Nichia Chemical Company, Japan. **Kingbright Company, USA. ***Fullbright Company, USA.

4.3.2.1 Dependence of stimulation wavelength on pulse-current

The dependence of stimulation wavelength on pulse-current of Nichia NSPB500AS blue LEDs was studied. A blue LED was pulsed at 11 μs at six different currents of 20, 36, 61, 85, 97 and 109 mA. Spectra corresponding to each current were measured with the Daedalon E0-85 spectrophotometer described earlier. The experiment was repeated five times for each pulse-current.

Figure 4.7 shows the LED peak emission wavelength as a function of pulse-current. The LED peak-wavelength shifts to shorter wavelengths with pulse-current. The peak-wavelength decreased from 470.0 $\pm$ 0.4 nm at 20 mA to 464.2 $\pm$ 0.4 at 109 mA. The complete results are shown in Table 4.2. Figure 4.8 shows a plot of LED intensity as a function of pulse-current. The intensity increases with increasing pulse-current. As the intensity increases, the peak-wavelength shifts to shorter wavelengths.

Figure 4.9 shows the full width at half maximum (FWHM) at various pulse-currents. The FWHM was unaffected by a change in pulse-current. The FWHM was constant at 25 nm between 20 and 109 mA . Thus, the curves only shift in position to shorter wavelengths whereas the FWHM was unaffected. These results are in agreement with those reported by Brown et al [33]. Brown et al. [33] studied the spectral emission properties of some blue LEDs. The blue light-emitting-diodes; NSPB500S, 110121 and 110039 were operated using 20 mA direct-current. These LEDs showed peak emission at wavelengths of 430, 450 and 470 nm and FWHM of 65, 78 and 28 nm, respectively. Brown et al. [33] reported no change in the FWHM for the blue NSPB500S LED when it was operated between 20 and 30 mA direct-current. In our study the FWHM of the blue NSPB500AS LED was constant between 20 and 109 mA pulse-currents. The blue NSPB500S LED studied by Brown et al. [33] and with the blue NSPB500AS LED studied in this project were manufactured by Nichia Chemical Company, Japan.

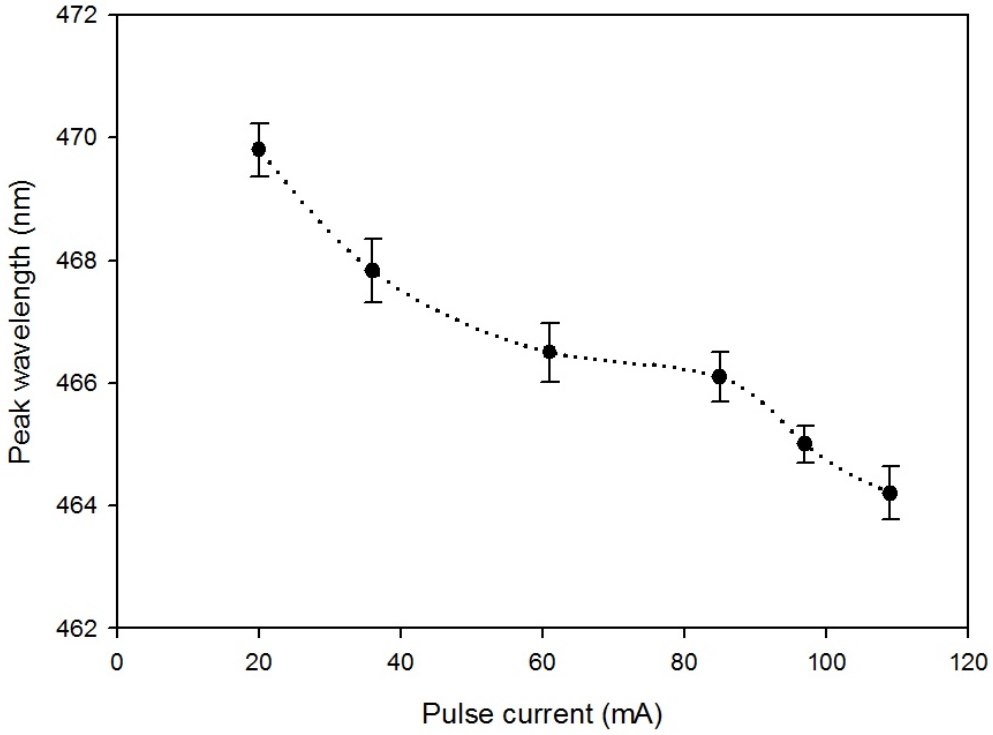

Figure 4.7: Peak-wavelength as a function of pulse-current. The dotted line is only a visual guide.

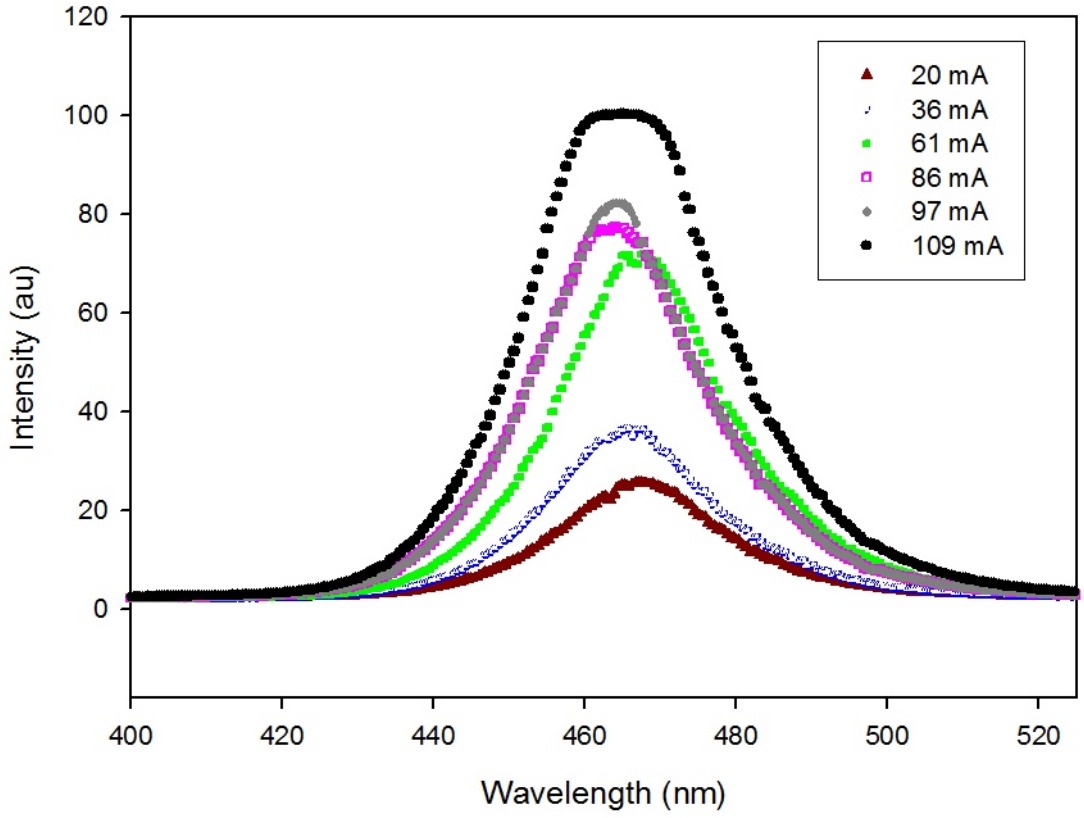

Figure 4.8: A plot of LED intensity against peak-wavelength. The curves show a shift in peak-wavelength to shorter wavelengths with increasing pulse-current.

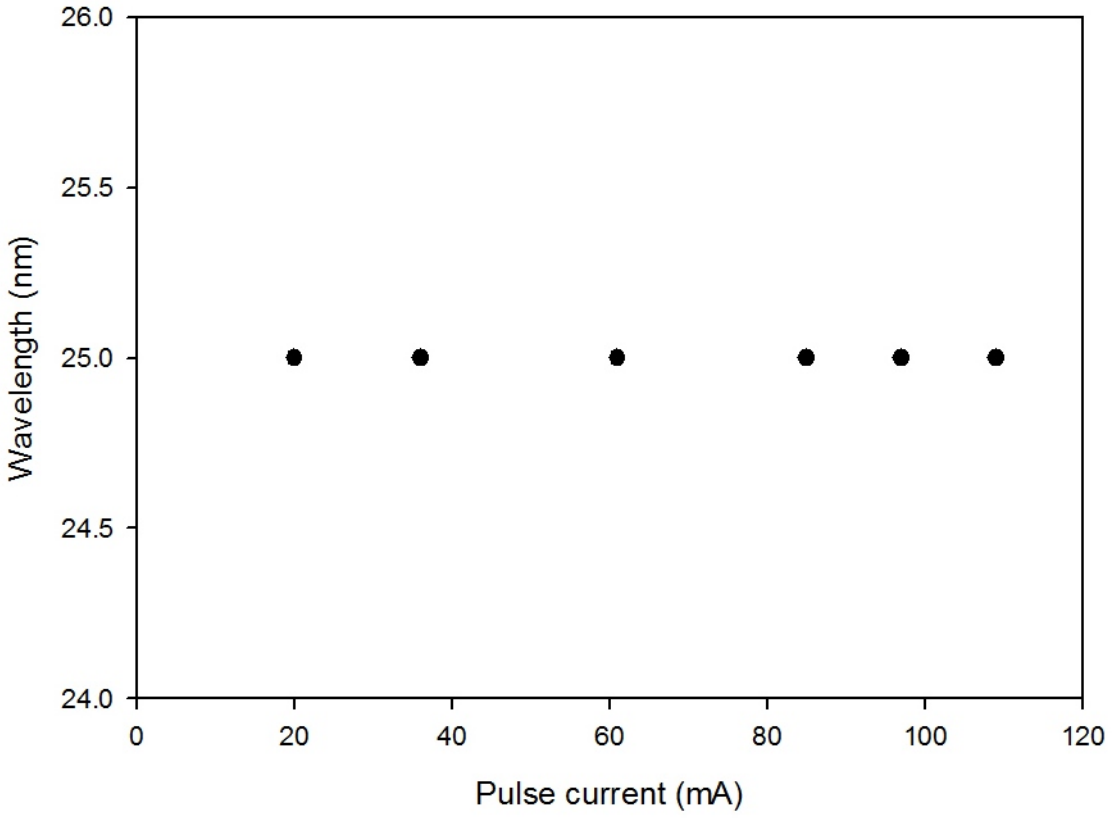

Figure 4.9: A plot of full-width at half maximum as a function of pulse-current.

Table 4.2: Peak-wavelength obtained at various pulse-currents.

Pulse-current (mA)	Peak-wavelength (nm)
20	470.0 ± 0.4
36	468.1 ± 0.5
61	466.5 ± 0.4
85	466.1 ± 0.4
97	465.0 ± 0.2
109	464.2 ± 0.4

Chapter 5

Applications

This chapter reports the application of the pulsing system to study TR-OSL spectra from quartz and α-Al_2O_3:C. The measurements reported here were made using the new pulsing system described in the previous chapters.

5.1 Time-resolved optically stimulated luminescence of quartz

Figure 5.1 shows an example of a TR-OSL spectrum obtained from a sample of quartz annealed at 500 ^{0}C and irradiated to 5 Gy. The luminescence was stimulated at a pulse width of 11 μs. The open circles represent the TR-OSL spectrum while the solid squares show background counts. The inset shows the portion of the TR-OSL spectrum after the light-pulse. All measurements were undertaken using the new pulsing system as described in section 4.2. Each measurement was repeated five times and the mean lifetime obtained. The portion of each TR-OSL spectrum after the light-pulse was fitted with the equation,

$$l(t) = A\exp(-\frac{t}{\tau}) + B, \tag{5.1}$$

where A is a scaling parameter, $\tau = \frac{1}{\lambda}$ is the luminescence lifetime, $l(t)$ is the time-dependence of luminescence after the light-pulse, t is time and B a constant added to account for the background signal. The luminescence lifetime extracted from the fit is 40.2 $\pm$ 2.0 μs. This value is consistent with ones reported for quartz annealed at 500 ^{0}C. For example, Galloway [30] reported a lifetime of 39.9 $\pm$ 0.4 μs for a sample of quartz annealed at 500 ^{0}C, Chithambo and Galloway [13] reported a lifetime of 40.0 $\pm$ 0.3 μs for quartz annealed at 500 ^{0}C and Chithambo [34] reported a lifetime of 41.8 $\pm$ 0.3 μs for quartz annealed at 500 ^{0}C. The luminescence lifetimes obtained using the new system are in good agreement with those reported in the literature as explained.

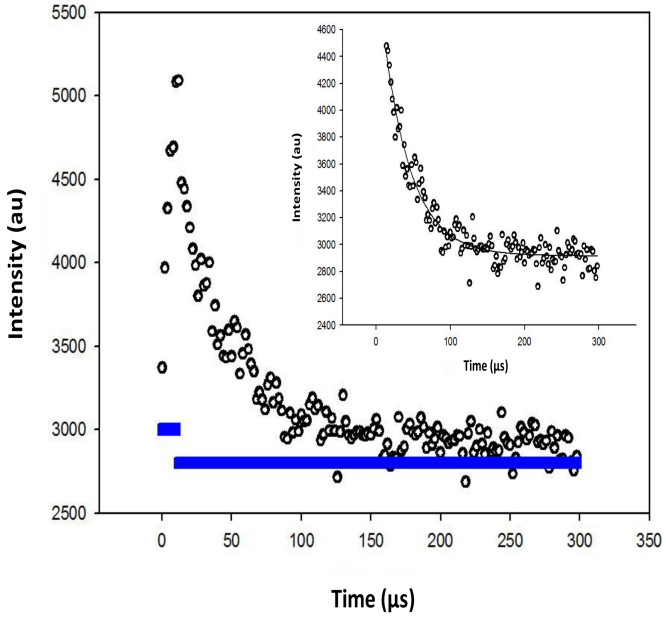

Figure 5.1: A TR-OSL spectrum from a sample of quartz annealed at 500 ^{0}C and irradiated to 5 Gy before 470 nm pulsed stimulation. Background counts (solid squares) are shown for comparison. The inset shows the luminescence after the light-pulse.

5.1.1 Dependence of luminescence lifetimes on dose

The aim of this experiment was to investigate the dependence of luminescence lifetimes on dose in quartz annealed at 500 ^{0}C. The sample was irradiated with beta doses between 5 and 200 Gy before 470 nm stimulation using an 11 μs pulse. Measurements were repeated

five times and the mean lifetime evaluated. Luminescence lifetimes were evaluated for each TR-OSL spectrum by fitting Equation 5.1 to the signal after the light-pulse.

Figure 5.2 shows the dependence of luminescence lifetimes on beta dose. For all doses used in this experiment, that is, between 5 and 200 Gy, the luminescence lifetimes obtained were unaffected by beta dose. The mean lifetimes were constant at about 42 $\pm$ 1.3 μs. Thus, our results show that luminescence lifetimes in quartz are independent of radiation dose for a sample annealed at 500 ^{0}C. This value is consisted with ones reported for quartz annealed at 500 ^{0}C. For example, Galloway [30] reported a lifetime of 41.5 $\pm$ 0.5 μs for quartz annealed at 500 ^{0}C and Chithambo [34] reported a lifetime of 41.8 $\pm$ 0.3 μs for quartz annealed at 500 ^{0}C.

The influence of irradiation on luminescence lifetimes can be described with reference to an energy band model proposed by Galloway [30]. Figure 5.3 shows this energy band model consisting of a non-radiative recombination centre R and three radiative centres labelled as L_H, L_L and L_S. The electron traps are shallow traps (ST), optically sensitive traps(LST) and deep traps which are not optically stimulated, represented as DT. In this model, annealing causes the transfer of holes from a non-radiative centre R to and between radiative centres L_H, L_L and L_S with corresponding lifetimes τ_H and τ_L [30]. All luminescence centre contribute to the stimulated luminescence but the value of the luminescence lifetime depends on the luminescence centre that is dominant [30].

The luminescence lifetime is independent of dose because most of the luminescence is emitted from L_H centres which would not have been sufficiently emptied by annealing at 500 ^{0}C prior to irradiation [24, 30].

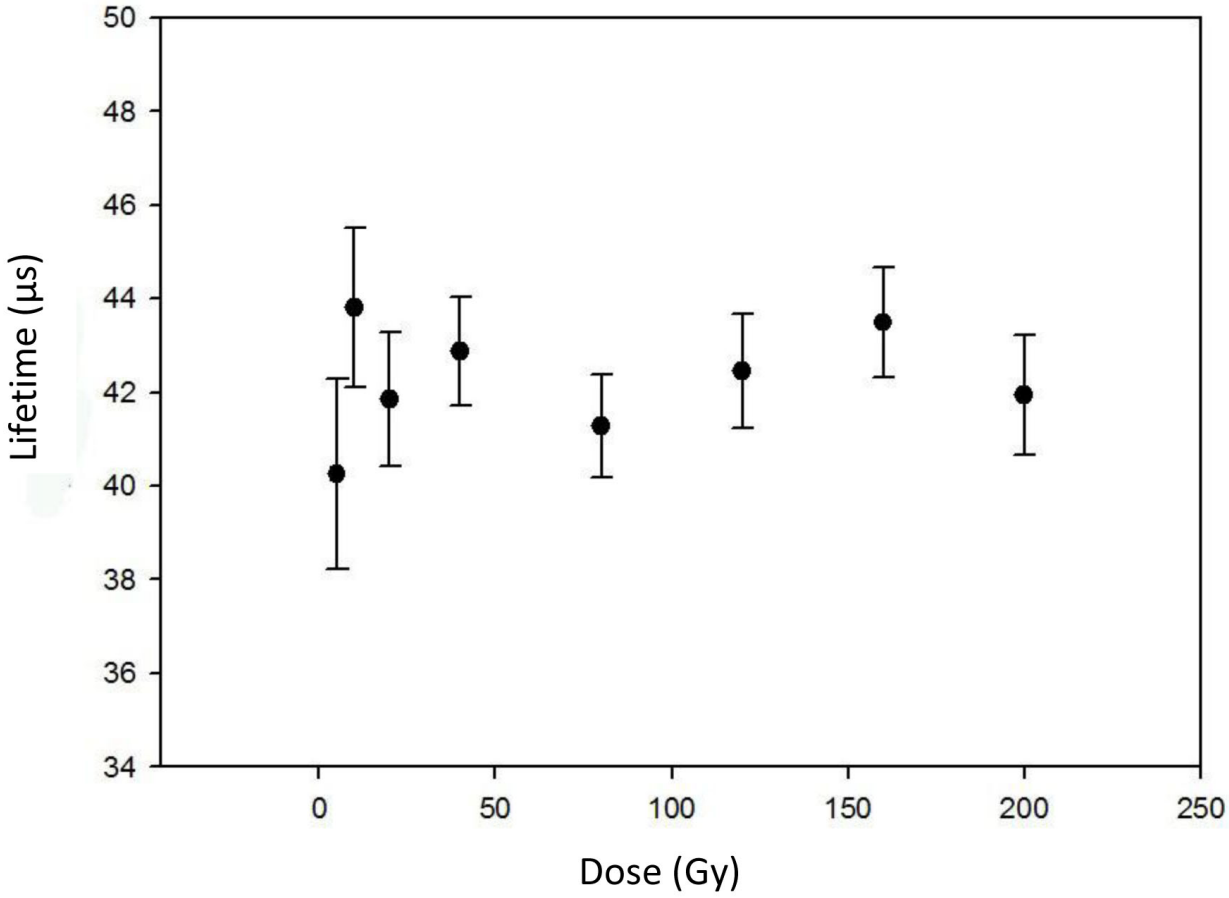

Figure 5.2: Dependence of luminescence lifetimes on beta dose in quartz annealed at 500 ^{0}C.

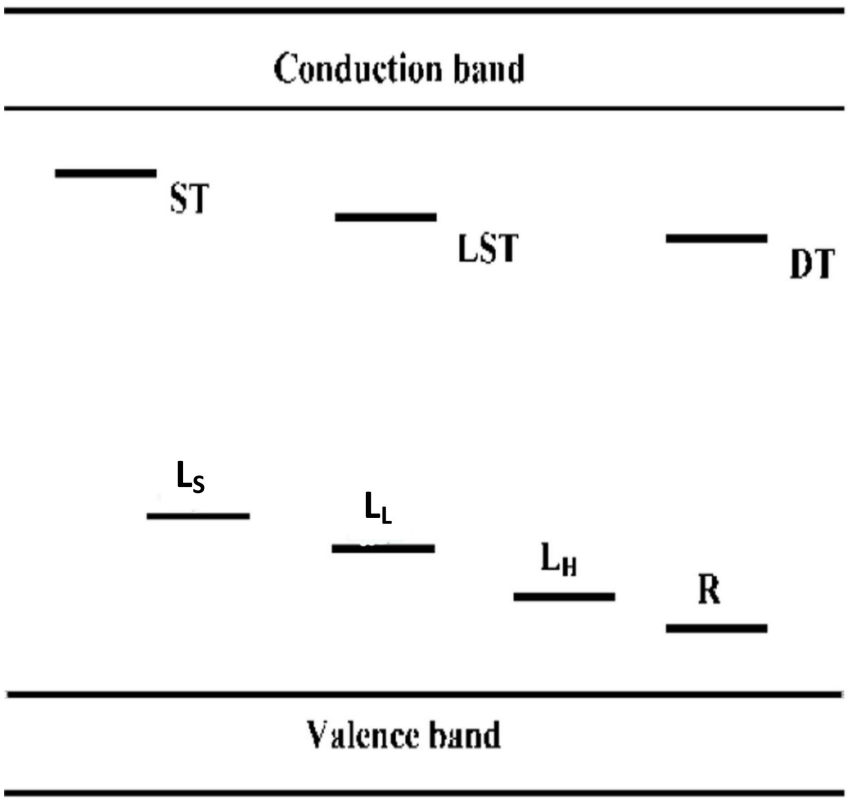

Figure 5.3: An energy band model used to describe dose dependence of luminescence lifetimes in quartz. The model consists of a non-radiative centre R; three radiative centres L_S, L_L and L_H, and three electron traps ST, LST and DT [30].

5.1.2 Dependence of luminescence lifetimes on measurement temperature

The effect of measurement temperature on luminescence lifetimes was investigated in quartz annealed at 500 ^{0}C. All measurements were made at 11 μs pulse-width, 90 mA pulse-current and a 300 μs dynamic range. Note that all data is described in degrees Celsius unless otherwise specified.

Figure 5.4 shows the dependence of luminescence lifetimes on measurement temperature from 20 to 200 ^{0}C represented in the figure as (heating) and from 200 to 20 ^{0}C denoted as (cooling) in steps of 20 ^{0}C, respectively. Luminescence lifetimes obtained from 20 to 100 ^{0}C were constant at about 40.4 $\pm$ 0.9 μs. Thereafter, the values decreased to a minimum

of 14.8 ± 1.8 μs at 200 ^{0}C. The decrease of the luminescence lifetimes with temperature is due to increased probability of non-radiative transitions at high temperature known as thermal quenching. Thermal quenching is the loss of luminescence efficiency with increasing temperature [1]. The change in luminescence lifetimes with increasing temperature as shown in Figure 5.4 is described by and was fitted with a thermal quenching equation of the form:

$$\tau = \frac{\tau_0}{1 + C\exp(-\frac{\Delta E}{kT})}, \tag{5.2}$$

where τ is the luminescence lifetime at any temperature T, τ_0 the luminescence lifetime at 0 K, C a constant, ΔE the activation energy of thermal quenching and k Boltzmann's constant [35]. From the fit, $\Delta E = 0.67 \pm 0.05$ eV; C $= 2 \times 10^7$ for measurements from 20 to 200 ^{0}C and $\Delta E = 0.72 \pm 0.03$ eV; C $= 1 \times 10^8$ for measurements from 200 to 20 ^{0}C. The two experimental values of ΔE agree within experimental error as expected since they refer to the same process. These results are also consistent with values of ΔE reported for samples of quartz annealed at 500 ^{0}C as reported in the literature for example, 0.66 ± 0.04 eV by Chithambo and Galloway [17] and 0.77 ± 0.06 eV by Galloway [30]. Values of ΔE are compared in Table 5.1.

Figure 5.5 shows a model used to explain thermal quenching in quartz. The model consists of one radiative centre and one non-radiative centre within the recombination centre. The model allows for non-radiative transitions into the ground state with thermal activation energy of quenching, ΔE [21, 23]. In this model electrons from a trap are raised by optical or thermal stimulation into the conduction band, followed by an electronic transition from the conduction band into an excited state of the recombination centre. Subsequently electrons in this excited state undergo either a direct radiative transition into a recombination centre, or a competing thermally assisted non-radiative process into the ground state of the recombination centre.

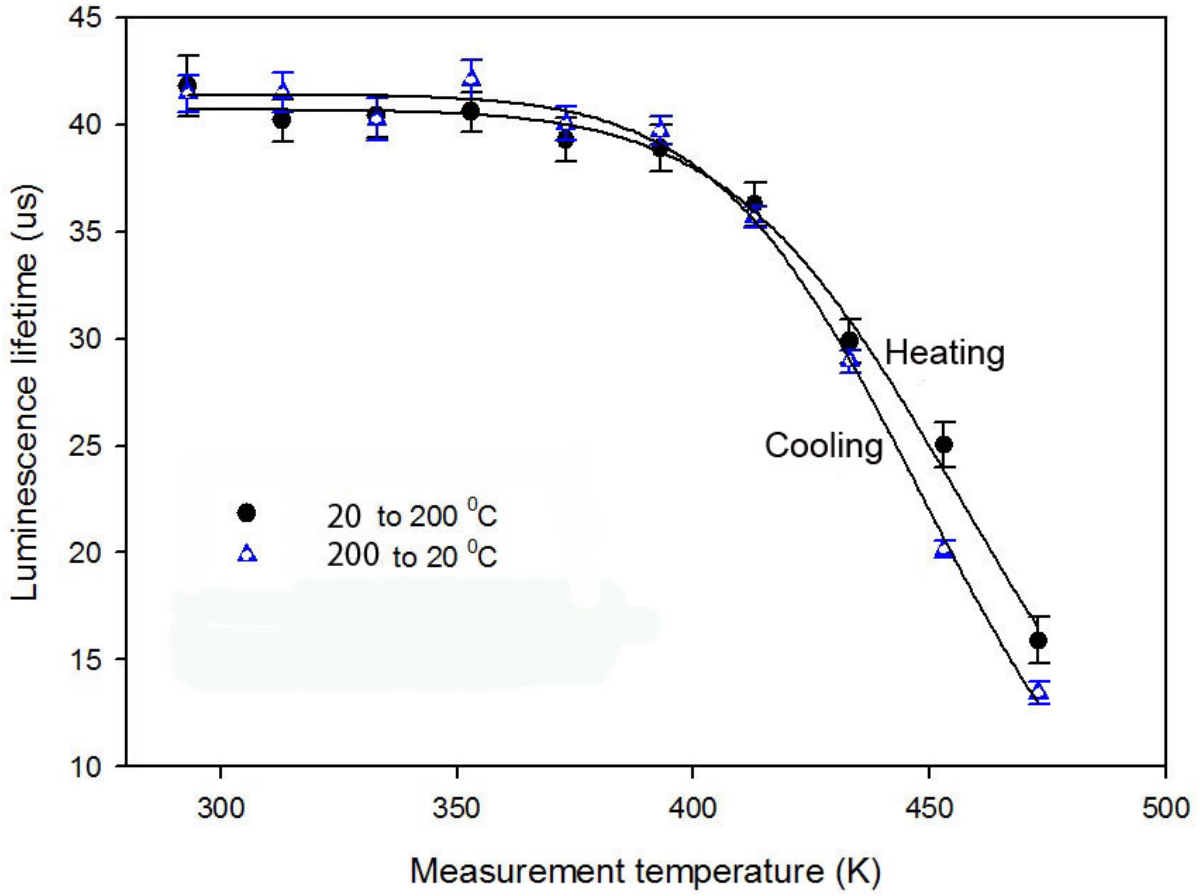

Figure 5.4: Dependence of luminescence lifetime on measurement temperature in quartz. The TR-OSL spectra were measured from 20 to 200 ^{0}C (a) and from 200 to 20 ^{0}C (b), in steps of 20 ^{0}C.

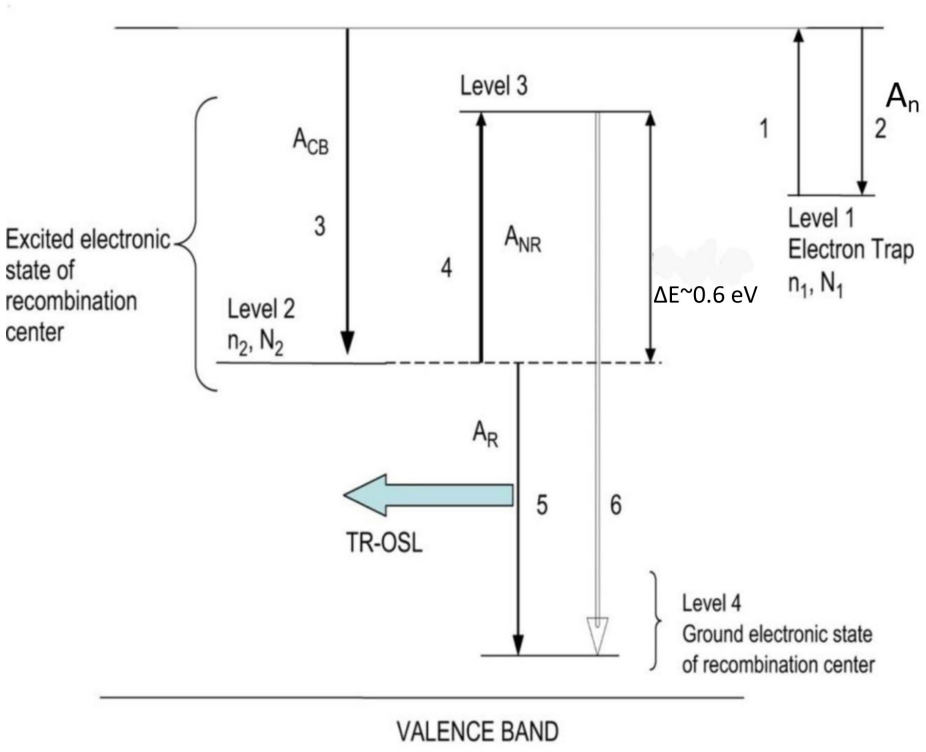

Figure 5.5: A model for thermal quenching in quartz. The model consists of an electron trap (level 1), two excited states within the radiative recombination center (levels 2 and 3), and the corresponding ground state (level 4) [21, 23].

Table 5.1: A list of values for the activation energy of thermal quenching, ΔE, obtained in this project and some reported in the literature.

Measurement temperature (^{0}C)	Radiation dose (Gy)	ΔE (eV)	C	Reference
20 to 200	80	0.67 ± 0.05	2x10^7	This work, figure 5.4
200 to 20	80	0.72 ± 0.03	1x10^8	This work, figure 5.4
20 to 200	4.5	0.64 ± 0.03	3 x 10^7	Chithambo and Galloway [17]
20 to 200	15	0.69 ± 0.79	8 x 10^7	Chithambo and Galloway [17]
20 to 200	150	0.66 ± 0.04	4 x 10^7	Chithambo and Galloway [17]
200 to 20	15	0.67 ± 0.05	5 x 10^7	Chithambo and Galloway [17]
200 to 20	150	0.58 ± 0.06	5 x 10	Chithambo and Galloway [17]
20 to 200	343	0.83 ± 0.01		Ogundare and Chithambo [19]

5.1.3 Dependence of luminescence intensity on measurement temperature

The effect of measurement temperature on luminescence intensity was investigated in quartz annealed at 500 ^{0}C. The intensity was obtained by integrating a time-resolved luminescence spectrum corresponding to each measurement temperature between 20 and 200 ^{0}C.

Figure 5.6 shows the dependence of luminescence intensity on measurement temperature. The intensity decreases with measurement temperature from 20 to 200 ^{0}C. When measurements are made from 200 to 20 ^{0}C, the intensity increases as the temperature is decreased. The change in intensity with measurement temperature in both cases is similar.

The change in intensity with measurement temperature as shown is attributed to thermal quenching and is described as

$$I(T) = \frac{I_0}{1 + C\exp(-\frac{\Delta E}{KT})}, \tag{5.3}$$

where I_0 denotes the initial value of luminescence intensity and the other parameters are as described previously [17, 36]. Thermal quenching is the result of increased probability of non-radiative transitions at high temperature.

The data shown in Figure 5.6 was fitted with Equation 5.3. From the fit, $\Delta E = 0.61 \pm 0.08$ eV; C = 7 x 10^7 for measurements from 20 to 200 ^{0}C and $\Delta E = 0.66 \pm 0.08$ eV; C = 7 x 10^7 for measurements from 200 to 20 ^{0}C. These results obtained for ΔE are consistent with those reported in the literature [17, 30, 36]. For example, Galloway [30] reported 0.72 ± 0.08 eV for ΔE for a sample of quartz annealed at 500 ^{0}C without preheating. Chithambo and Galloway [17] reported 0.68 ± 0.11 eV for ΔE when the temperature increased from 20 to 200 ^{0}C and 0.57 ± 0.08 eV when the temperature was decreased from

200 to 20 ^{0}C for quartz.

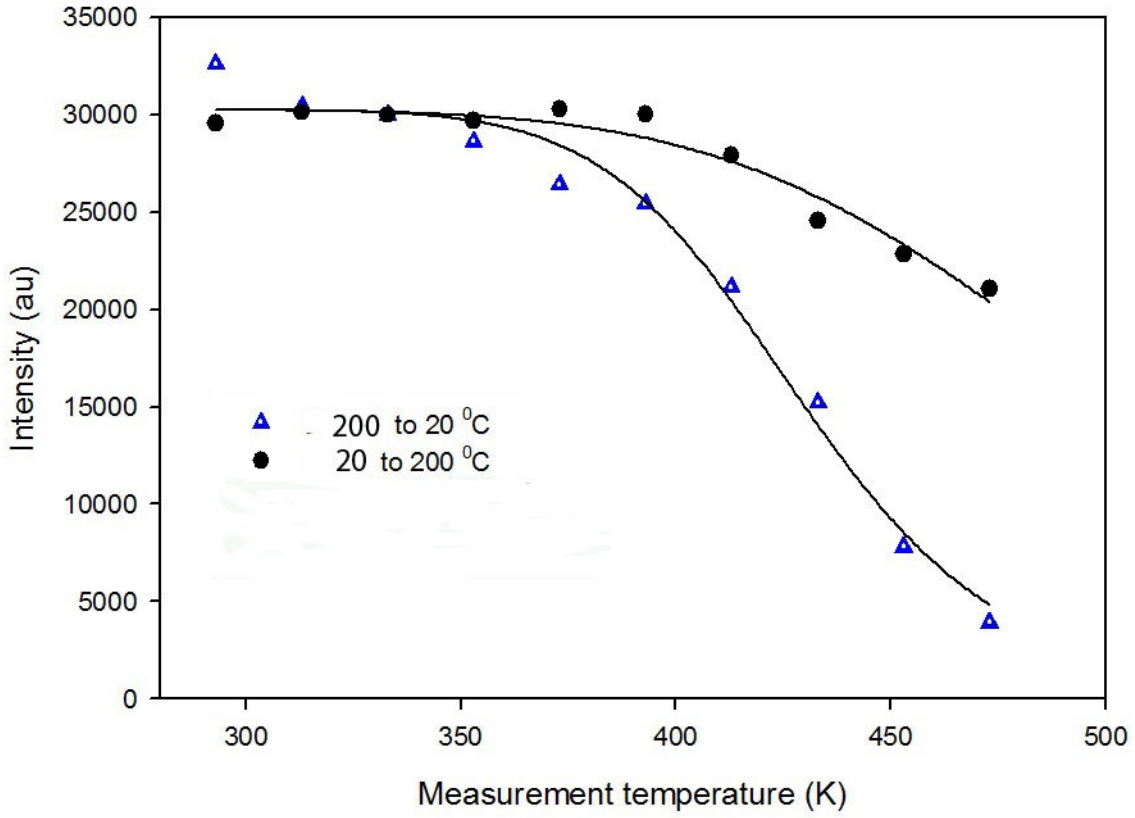

Figure 5.6: Dependence of luminescence intensity on measurement temperature in quartz annealed at 500 ^{0}C and irradiated to 80 Gy. Measurements were made from 20 to 200 ^{0}C and from 200 to 20 ^{0}C, in steps of 20 ^{0}C, respectively.

5.2 Time-resolved luminescence from α-Al_2O_3:C

This section reports investigations on the dependence of luminescence lifetimes on measurement temperature in carbon-doped aluminium oxide, α-Al_2O_3:C, a highly sensitive luminescence dosimeter. The sample used was irradiated to 1.0 Gy before 470 nm pulsed stimulation. The luminescence was stimulated at a 17 ms pulse-width using 150 ms dynamic range. TR-OSL spectra were measured from 20 to 140 ^{0}C in steps of 20 ^{0}C.

Figure 5.7 shows an example of a TR-OSL spectrum obtained from α-Al_2O_3:C following beta irradiation to 1.0 Gy. Measurements were made at 40 and 140 ^{0}C. The solid squares in

the figure show the background counts. The inset shows the portion after the light-pulse.

The portion after the light-pulse was analysed using Equation 5.1 to give the associated luminescence lifetime at a particular temperature. A luminescence lifetime of 35.5 ± 0.5 ms was obtained from the fit in Figure 5.7 (inset).

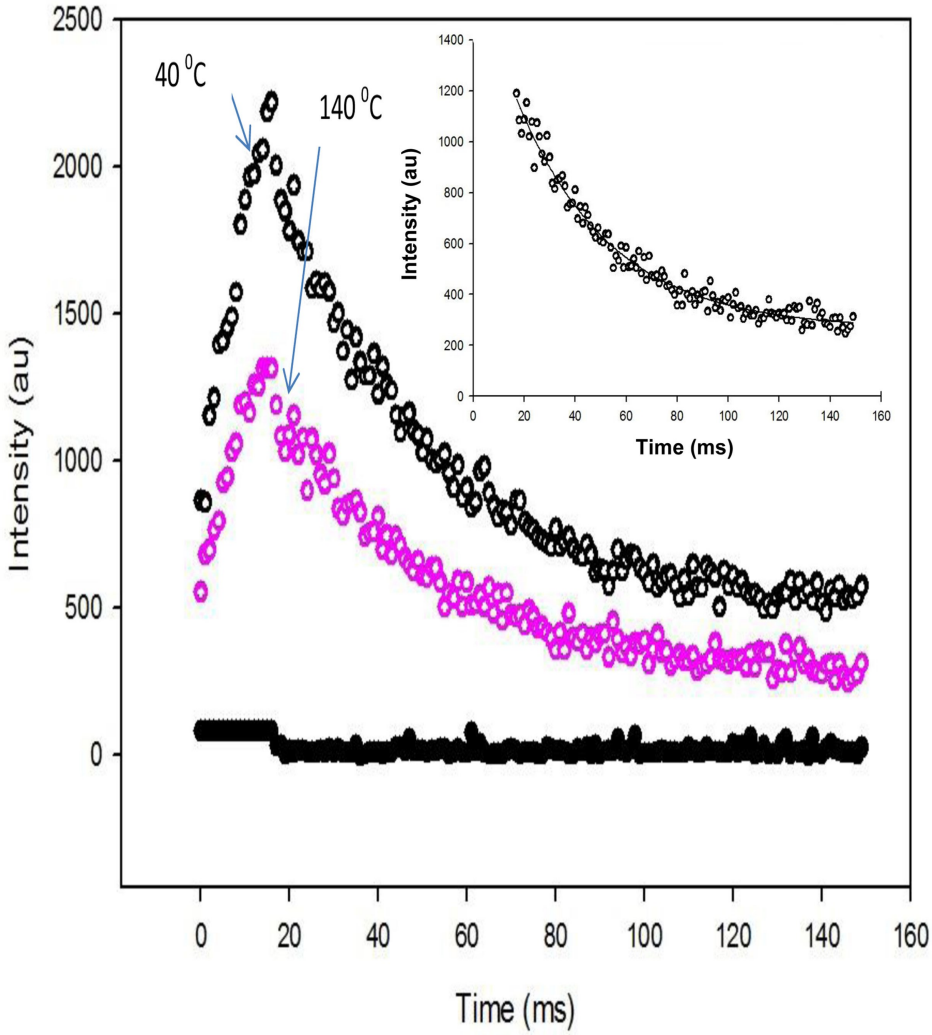

Figure 5.7: A TR-OSL spectrum from a sample of α-Al_2O_3:C following beta irradiation to 1 Gy. Measurements were made at 40 and 140 ^{0}C. Background counts (solid squares) are also shown. The inset shows the portion after the light-pulse.

Figure 5.8 shows the dependence of luminescence lifetimes on measurement temperature. The experiment was conducted at measurement temperatures from 20 to 140 ^{0}C in steps of 20 ^{0}C. Luminescence lifetimes from 20 to 60 ^{0}C were constant at about 36.8 ± 0.1

ms. Thereafter, the values decreased to a minimum of 28.0 ± 0.6 ms at 140 ^{0}C. This decrease in luminescence lifetime is evidence of thermal quenching. The luminescence lifetime decreases as a function of temperature as described before as

$$\tau = \frac{\tau_0}{1 + C\exp(-\frac{\Delta E}{KT})} \tag{5.4}$$

where all parameters are as described previously. The data in Figure 5.8 was fitted with Equation 5.4, and the values of ΔE and C obtained from the fit are 1.02 ± 0.01 eV and 9 × 10^{11} respectively. The value of ΔE is in good agreement with 1.08 ± 0.03 eV reported by Akselrod et al. [35], 1.075 ± 1.0 eV reported by Pagonis et al. [27], 0.96 ± 0.005 eV reported by Ogundare et al. [37] and 0.95 ± 0.04 eV by Chithambo et al. [38].

Thermal quenching is a process caused by loss of luminescence efficiency. Nikiforov et al [39] developed a model that describes thermal quenching in α-Al_2O_3:C based on thermal and optical ionization of F-centres. However, in this thesis, thermal quenching in α-Al_2O_3:C is described in terms of the model of Pagonis et al. [40]. Figure 5.9 shows the model of Pagonis et al. [40] for thermal quenching in α-Al_2O_3:C. This model consists of an electron trap, two deep traps, and excited levels of the F-centre. The model allows non-radiative transition into the ground state with thermal activation energy of quenching, ΔE. Pagonis et al [40] described thermal quenching based on competition between radiative and non-radiative electronic transitions occurring within the recombination centre. The electrons from the trap are stimulated by optical or thermal stimulation into the conduction band. The electrons then transit from the conduction band into an excited state of the recombination centre. Subsequently electrons in this excited state undergo either a direct radiative transition into a recombination centre, or a competing thermally assisted non-radiative process into the ground state of the recombination centre. During this non-radiative transition into the ground state of the recombination centre, the absorbed energy is released as phonons.

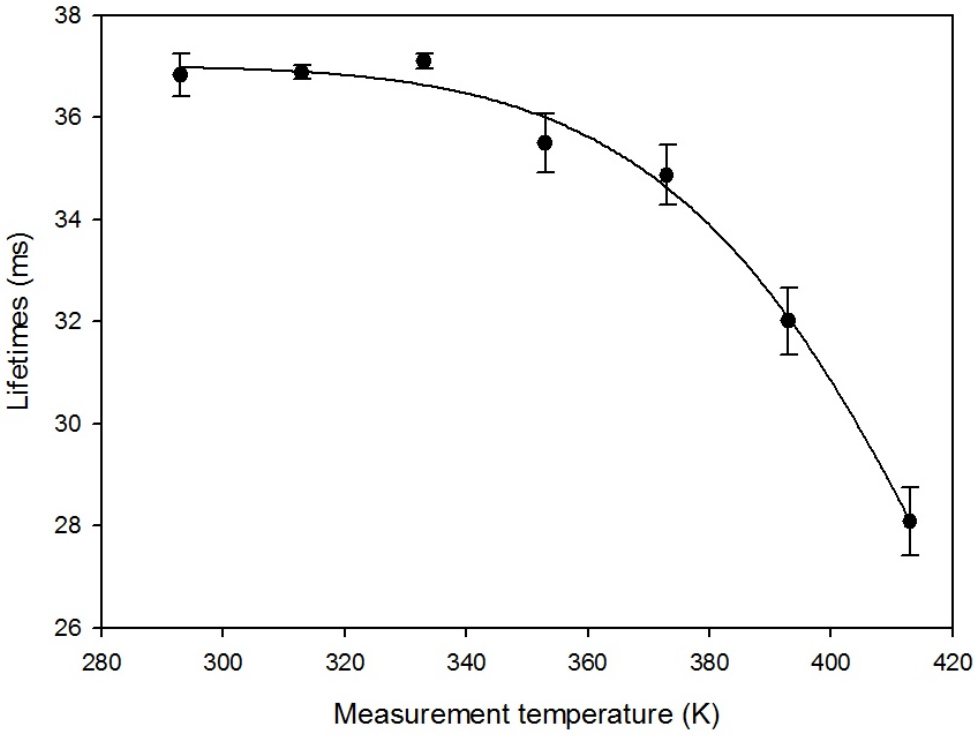

Figure 5.8: Dependence of luminescence lifetimes on measurement temperature in α-Al_2O_3:C following beta irradiation to 1 Gy. All measurements were made from 20 to 140 ^{0}C in steps of 20 ^{0}C.

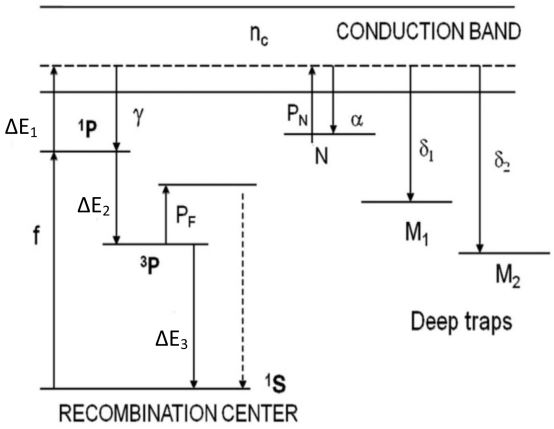

Figure 5.9: An energy band model used to describe thermal quenching based on competition between radiative and non-radiative electronic transitions occurring within the recombination centre in α-Al_2O_3:C [40].

Chapter 6

Conclusion

A new light-emitting-diode based pulsing system for measurement of TR-OSL has been developed. The pulsing system is designed to generate pulses of various duration and, stimulation power. The light-emitting-diodes are pulsed at various duration by a 555-timer integrated circuit operated as a monostable multivibrator. The LEDs are connected in parallel in sets of four, each containing four LEDs in series.

The pulsing circuitry is made up of a 555-timer which produces pulses of different widths. The output-pulse obtained from the 555-timer is fed into the gate-pin of an 2N7000 MOSFET which then supplies sufficient pulse-current to the LEDs. In the pulsing circuitry, the source-pin of the 2N7000 is earthed while the drain-pin is connected to the LEDs. The 2N7000 MOSFET is used as a switch to increase the pulse-current obtained from the NE555N timer. The 2N7000 can switch a maximum pulse-current of 500 mA, with a maximum ON-resistance of 5 ohm at 4.5 V Vgs. A multichannel scaler was used to trigger the pulsing circuitry. The circuitry is capable of generating pulse-widths in the range of microseconds upwards. The stimulation power of the LEDs is controlled and regulated by an integrated adjustable power supply (EPS-3250) of constant current. The emitted luminescence is detected by a photomultiplier tube (EMI 9635QA).

Blue NSPB500AS LEDs were used as stimulation light-sources. The dependence of the emission peak-wavelength on pulse-current of the blue LEDs were investigated. The peak-wavelength decreased with increasing pulse-current from 470.0 ± 0.4 nm at 20 mA to 464.4 ± 0.4 nm at 109 mA.

TR-OSL spectra from two major dosimetric materials, quartz and α-Al_2O_3:C were measured to demonstrate the system performance. TR-OSL was measured at beta doses between 5 and 200 Gy from a sample of quartz to investigate the dependence of luminescence lifetimes on dose. The luminescence lifetimes obtained were independent of beta dose between 5 and 200 Gy. The luminescence lifetime is independent of dose because most of the luminescence is emitted from L_H centres which would not have been sufficiently emptied by annealing at 500 ^{0}C prior to irradiation [24]. In addition, TR-OSL was measured at various temperatures from 20 to 200 ^{0}C and from 200 to 20 ^{0}C in steps of 20 ^{0}C, respectively for a sample of quartz annealed at 500 ^{0}C. The luminescence lifetime showed evidence of thermal quenching as the measurement temperature increased. The activation energy of thermal quenching ΔE obtained for the quartz sample was 0.67 ± 0.05 eV for measurements from 20 to 200 ^{0}C. When the temperature was decreased from 200 to 20 ^{0}C, the value of ΔE obtained was 0.72 ± 0.03 eV. These values of ΔE are in good agreement with each other and with others reported in the literature for example, 0.66 ± 0.04 eV by Chithambo and Galloway [17] and 0.77 ± 0.06 eV by Galloway [30].

The dependence of luminescence lifetimes on measurement temperature were studied in α-Al_2O_3:C. TR-OSL was measured at various temperatures from 20 to 140 ^{0}C in steps of 20 ^{0}C. The luminescence lifetimes showed evidence of thermal quenching as the measurement temperature increased. The activation energy of thermal quenching ΔE obtained for α-Al_2O_3:C was 1.02 ± 0.01 eV. The value of ΔE is in good agreement with those reported in the literature for example 1.08 ± 0.03 eV by Akselrod et al. [35], 1.075 ± 1.0 eV reported by Pagonis et al. [27], 0.96 ± 0.005 eV reported by Ogundare et al. [37] and

0.95 ± 0.04 eV by Chithambo et al. [38]. Hence, a new light-emitting-diode based pulsing system for measurement of TR-OSL has been developed. The performance of the new pulsing system from TR-OSL measurements on quartz and α-Al_2O_3:C agrees with values of lifetime studied with other systems in the literature.

6.1 Recommendations

The pulsing system is capable of producing pulses of various widths from microseconds upwards, for example, microseconds pulse-widths for quartz and milliseconds pulse-widths for α-Al_2O_3:C. This system offers an improved settability of the various pulses and, stimulation power. Future studies can focus on the use of a micro-controller to produce pulses of various widths. The use of a micro-controller will also enable digital control of output pulses from the computer. By using a micro-controller, stable pulses of various widths can be obtained.

References

[1] L. Botter-Jensen, S.W.S. McKeever and A.G. Wintle. *Optically stimulated luminescence dosimetry*. Elsevier, Amsterdam, 2003.

[2] V. Pagonis, G. Kitis and C. Furetta. *Numerical and practical exercises in thermoluminescence*. Springer, New York, 2006.

[3] S.W.S. McKeever. *Thermoluminescence of solids*. Cambridge University Press, Cambridge, 1988.

[4] L. Botter-Jensen. *Development of optically stimulated luminescence techniques using natural minerals and ceramics, and their application to retrospective dosimetry*. PhD thesis, University of Copenhagen and Riso National Laboratory, Roskilde, 2000.

[5] E. G. Yukihara and S. W. S. McKeever. *Optically stimulated luminescence: Fundamentals and applications*. Wiley, 2011.

[6] L. Botter-Jensen and G.A.T. Duller. A new system for measuring OSL from quartz samples. *Nucl. Tracks Rad. Meas*, 20 : 549 – 553, 1992.

[7] L. Botter-Jensen and A.S. Murray. Optically stimulated luminescence techniques in retrospective dosimetry. *Radiat. Phys. Chem*, 61 : 181 – 190, 2001.

[8] E. Bulur. An alternative technique for optically stimulated luminescence (OSL) experiment. *Radiat. Meas*, 26 : 701 – 709, 1996.

[9] M.L. Chithambo. A time-correlated photon counting system for measurement of pulsed optically stimulated luminescence. *J. Lumin*, 131 : 92 – 98, 2011.

[10] D.C.W. Sanderson and R.J. Clark. Pulsed photostimulated luminescence of alkali feldspars. *Radiat. Meas*, 23 : 633 – 639, 1994.

[11] B.G. Markey, L.E. Colyott and S.W.S. Mckeever. Time-resolved optically stimulated luminescence from α-Al_2O_3:C. *Radiat. Meas*, 24 : 457 – 463, 1995.

[12] S.W.S. McKeever, M.S. Akselrod and B.G. Markey. Pulsed optically stimulated luminescence dosimetry using α-Al_2O_3:C. *Radiat. Prot. Dosim*, 65 : 267 – 272, 1996.

[13] M.L Chithambo and R.B Galloway. A pulsed light-emitting-diode system for stimulation of luminescence. *Meas. Sci. Technol*, 11 : 418 – 424, 2000.

[14] M.L. Chithambo. The analysis of time-resolved optically stimulated luminescence: 1. Theoretical considerations. *J. Phys. D: Appl. Phys*, 40 : 1874 – 1879, 2007.

[15] M.L. Chithambo. The analysis of time-resolved optically stimulated luminescence: II. Computer simulations and experimental results. *J. Phys. D: Appl. Phys*, 40 : 1880 – 1889, 2007.

[16] V.H. Whitley and S.W.S. McKeever. Linearly modulated photoconductivity and linearly modulated optically stimulated luminescence measurements on α-Al_2O_3:C. *J. Appl. Phys*, 90 : 6073 – 6083, 2001.

[17] M.L. Chithambo and R.B. Galloway. On the slow component of luminescence stimulated from quartz by pulsed blue-light-emitting diodes. *Nucl. Instrum. Meth. B*, 183 : 358 – 368, 2001.

[18] F. Preusser, M.L. Chithambo, T. Gotte, M. Martini, K. Ramseyer, E.J. Sendezera, G.J. Susino and A.G. Wintle. Quartz as a natural luminescence dosimeter. *Earth-Sci. Rev*, 97 : 184 – 214, 2009.

[19] F.O. Ogundare and M.L. Chithambo. Time resolved luminescence of quartz from Nigeria. *Opt. Mater*, 29 : 1844 – 1851, 2007.

[20] S. W. S. McKeever and M. S. Akselrod. Radiation dosimetry using pulsed optically stimulated luminescence of α-Al_2O_3:C. *Radiat. Prot. Dosim*, 84 : 317 – 320, 1999.

[21] V. Pagonis, J. Lawless, R. Chen and M.L. Chithambo. Analytical expressions for time-resolved optically stimulated luminescence experiments in quartz. *J. Lumin*, 131 : 1827 – 1835, 2011.

[22] V. Pagonis, S.M. Mian, M.L. Chithambo, E. Christensen and C. Barnold. Experimental and modelling study of pulsed optically stimulated luminescence in quartz, marble and beta irradiated salt. *J. Phys. D: Appl. Phys*, 42 : 055407, 2009.

[23] V. Pagonis, C. Ankjaergaard, A.S. Murray, M. Jain, R. Chen, Lawless and S. Greilich. Modelling the thermal quenching mechanism in quartz based on time-resolved optically stimulated luminescence. *J. Lumin*, 130 : 902 – 909, 2010.

[24] M.L. Chithambo and F.O. Ogundare. Luminescence lifetime components in quartz: Influence of irradiation and annealing. *Radiat. Meas*, 44 : 453 – 457, 2009.

[25] M.L. Chithambo, F.O. Ogundare and J. Feathers. Principal and secondary luminescence lifetime components in annealed natural quartz. *Radiat. Meas*, 43 : 1 – 4, 2008.

[26] M.S. Akselrod and S.W.S. McKeever. A radiation dosimetry method using pulsed opticallly stimulated luminescence. *Radiat. Prot. Dosim*, 81 : 167 – 176, 1999.

[27] V. Pagonis, C. Ankjaergaard, M. Jain and R. Chen. Thermal dependence of time-resolved blue light stimulated luminescence in α-Al_2O_3:C. *J. Lumin*, 136 : 270 – 277, 2013.

[28] M.L. Chithambo, F. Preusser, K. Ramseyer and F.O. Ogundare. Time-resolved luminescence of low sensitivity quartz from crystalline rocks. *Radiat. Meas*, 42 : 205 – 212, 2007.

[29] V. Pagonis, M.L. Chithambo, R. Chen, A. Chruscinska, M. Fasoli, S.H. Li, M. Martini and K. Ramseyer. Thermal dependence of luminescence lifetimes and radioluminescence in quartz. *J. Lumin*, 145 : 38 – 48, 2014.

[30] R.B. Galloway. Luminescence lifetimes in quartz: dependence on annealing temperature prior to beta irradiation. *Radiat. Meas*, 35 : 67 – 77, 2002.

[31] M.L Chithambo. Procedures preparatory to setting up a luminescence pulsing system. *Ancient TL*, 23:39 – 42, 2005.

[32] *ORTEC datasheets,* ***http://www.ortec-online.com/Products-Solutions/Modular-Electronic-Instruments-Amplifiers.aspx***.

[33] S.W. Brown, J. Casswell, R.B. Galloway, S. Haddon and A. Moffat. Spectra emission properties of some blue light-emitting-diodes. *Ancient TL*, 17 : 1 – 4, 1999.

[34] M.L. Chithambo. On the correlation between annealing and variabilities in pulsed-luminescence from quartz. *Radiat. Meas*, 41 : 862 – 865, 2006.

[35] M.S. Akselrod, N.A. Larsen, V. Whitley and S.W.S. McKeever. Thermal quenching of F-center luminescence in α-Al_2O_3:C. *J. Appl. Phys*, 84 : 3364, 1998.

[36] A.S. Murray and A.G. Wintle. Factors controlling the shape of the OSL decay curve in quartz. *Radiat. Meas*, 29 : 65 – 79, 1998.

[37] F.O. Ogundare, S.A. Ogundele, M.L. Chithambo and M.K. Fasasi. Thermoluminescence characteristics of the main glow peak in α-Al_2O_3:C exposed to low environmental-like radiation doses. *J. Lumin*, 139 : 143 – 148, 2013.

[38] M.L. Chithambo, C. Seneza and F.O. Ogundare. Kinetic analysis of high temperature secondary thermoluminescence glow peaks in α-Al_2O_3:C. *Radiat. Meas*, 66 : 21 – 30, 2014.

[39] S.V. Nikiforov, I.I. Milman and V.S. Kortov. Thermal and optical ionization of F-centers in the luminescence mechanism of anion-defective corundum crystals. *Radiat. Meas*, 33 : 547 – 551, 2001.

[40] V. Pagonis, R. Chen, W. Maddrey and B. Sapp. Simulations of time-resolved photoluminescence experiments in α-Al_2O_3:C. *J. Lumin*, 131 : 1086 – 1094, 2011.

[41] W. Kleitz. *Digital Electronics*. Pearson, New Jersey, 2012.

Appendices

Appendix A

Components used in designing the pulsing system

A.1 NE555N timer

The NE555N timer is a stable integrated circuit capable of functioning as an accurate time-delay generator and as a free running multivibrator. The NE555N was used in this project as a pulse generator to produce pulses required to operate the LEDs used as luminescence stimulating light sources. The NE555N timer offers timing that ranges from microseconds to hours. When used as a pulse generator as in this case, the pulse-width is set externally by a combination of a resistor and a capacitor. The NE555N timer may be triggered and reset on a falling waveform. Some of the prominent features of the NE555N timer include a high current output of 200 mA, a logic compatible trigger, a reset feature and, an output operated in normal ON and OFF states.

Figure A.1 is a schematic diagram of an NE555N timer showing various pin connections. The pins are designed for different operation (Table A.1).

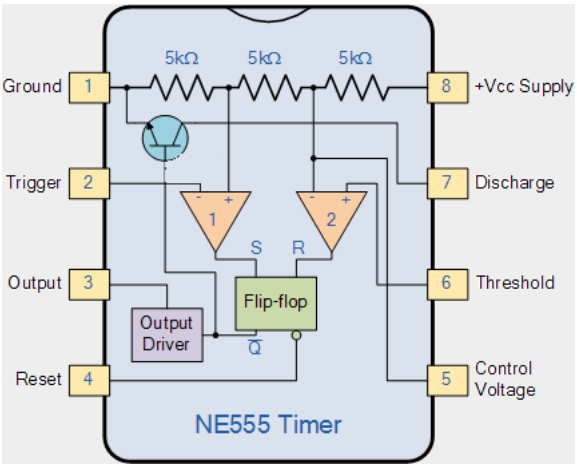

Figure A.1: Schematic block circuit diagram of the NE555N timer showing various pin connections. The numbers on the side are pins with their purpose as shown [41].

Table A.1: Pins on an NE555N timer and their associated functions.

Pin	Name	Function
1	Ground	Ground reference voltage (0 V)
2	Trigger	Starts the 555 running when triggered and causes the output to go HIGH
3	Output	Generates the output pulse
4	Reset	Resets the output of the timer to LOW
5	Control	Provides control access to the timer (usually connected to 0.01 μF to bypass noise
6	Threshold	Responsible for the timing capacitor charging
7	Discharge	Discharges the capacitor after a complete cycle
8	Vcc	Positive supply voltage usually from 5 V to 15 V

A.2 2N7000 MOSFET TRANSISTOR

The 2N7000 MOSFET is an N-channel, enhancement-mode MOSFETs used for low-power switching applications. The 2N7000 MOSFET was used to increase the output pulse-

current from the NE555N timer. In other words, the 2N7000 was used as a switch to moderate voltages and currents from the NE555N timer. The 2N7000 MOSFET is capable of switching a maximum pulse-current of 500 mA. This current is sufficient to drive the light-emitting-diodes (LEDs). Figure A.2 is a diagram of the 2N7000 MOSFET. Figure A.2(a) shows the electronic symbol whereas Figure A.2(b) shows the physical structure of the 2N7000. Pin 1 is the source, pin 2 the gate, and pin 3 the drain. Specifications of the 2N7000 MOSFET as given by the manufacturer (MOTOROLA) are given in Table A.2 as shown below:

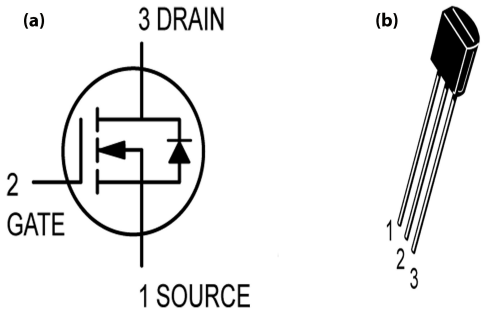

Figure A.2: A schematic diagram showing the electronic symbol of the 2N7000 MOSFET (a) and the physical structure of the 2N7000 (b).

Table A.2: The maximum absolute rating for an 2N7000 MOSFET [a]

Rating	Symbol	Value	Units
Drain source voltage	V_{DSS}	60	Vdc
Drain-Gate Voltage	V_{DGR}	60	Vdc
Gate-Source Voltage			
-Continous	V_{GS}	20	Vdc
-Non-repetetive	V_{GSM}	40	Vpk
Drain Current			
Continous	I_D	200	mAdc
Pulse	I_{DM}	500	
Total Power Dissipation @ Tc = 25 ^{0}C	P_D	350	mW
Above 25 ^{0}C		500	mW/^{0}C

[a]Motorola 2N7000 datasheet, `http://www.alldatasheet.com/datasheet-pdf/pdf/2842/MOTOROLA/2N7000.html`

A.3 Potentiometer

A potentiometer is a variable resistor containing three pins. By turning the shaft of the potentiometer, the resistance value changes. The potentiometer used in this project has resistance ranging between 0 and 500 kΩ. Figure A.3 shows how the potentiometer was used in the pulsing system. Figure A.3(a) shows the position of the potentiometer on the pulsing system connected to a fixed capacitor and A.3(b) shows the electronic symbol of the potentiometer. This type of connection enables the automatic control of the width of the output-pulse as shown earlier in Figure 4.3.

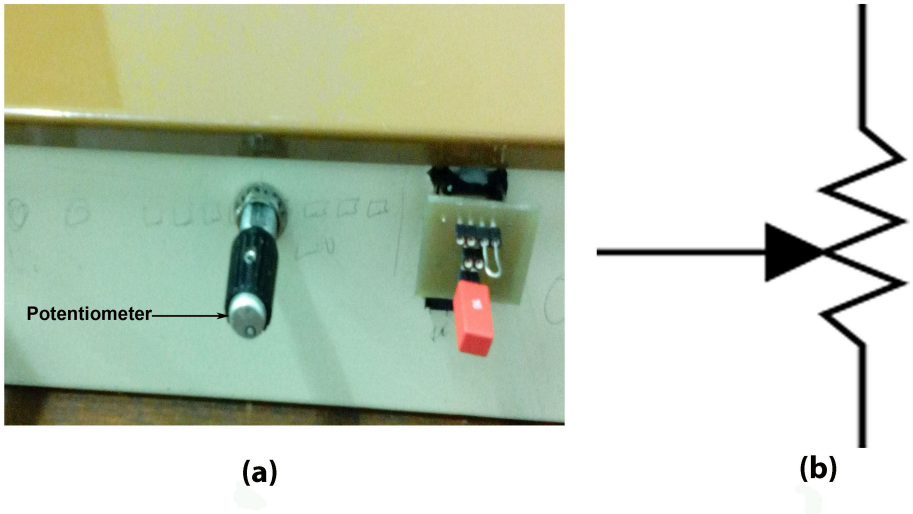

Figure A.3: A diagram showing how the potentiometer was used as shown earlier in Figure 4.3. Figure A.3(a) shows the potentiometer on the front plate of the chasis and Figure A.3(b) shows the electronic symbol of potentiometer.

A.4 Light-emitting-diodes

Sixteen blue light-emitting-diodes (Nichia NSPB500AS) were used as stimulation light sources. The NSPB500AS blue LED has a peak emission wavelength at 470 nm. The maximum rating specified for the LED by the manufacturer (Nichia Chemical Company, Japan) is 110 mA pulse-current and 30 mA direct-current. The 16 LEDs are connected in parallel in sets of four, each set containing four LEDs in series. Figure A.4(a) shows the

physical connection of a set of LEDs in series whereas Figure A.4(b) shows the electronic symbol of an LED. The full specifications of the Nichia NSPB500AS blue LED are shown in Table A.3.

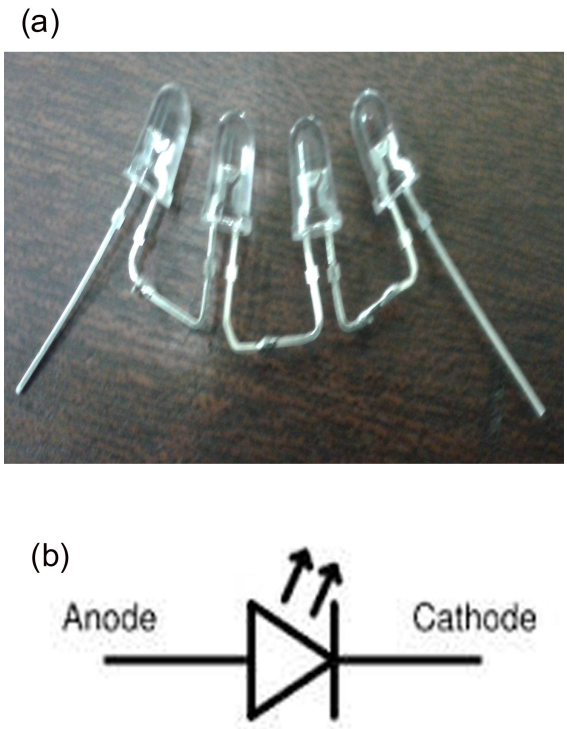

Figure A.4: A diagram showing the connection and the electronic symbol of an LED. A connection of one set of the NSPB500AS blue LEDs containing four LEDs in serial (a) and, the electronic symbol of an LED (b).

Table A.3: The specifications for Nichia NSPB00AS blue LED [a]

Item	Symbol	Rating	Unit
Forward Current	I_F	35 (absolute maximum) 20 (normal test condition)	mA
Pulse Forward Current	I_{FP}	110 (absolute maximum)	mA
Reverse Voltage	V_T	5 (absolute maximum)	mA
Forward Voltage	V_F	3.2 (if I_F = 20 mA) 3.5 (absolute maximum)	V
Power Dissipation	P_D	123 (absolute maximum)	mW
Luminous Intensity	I_V	11000 (if I_F = 20 mA)	mcd
Viewing angle		15	^{0}C
Dominant wavelength		470	nm

[a] http://www.alldatasheet.com/datasheet-pdf/pdf/240262/NICHIA/NSPB500AS.html

A.5 Copper etching of the pulsing circuitry board

Figure A.5 shows a single sided layer etched board of the pulsing system. The copper was etched in a system-designed tank containing cupric chloride solution ($CuCl_2$) and Hydrochloric acid (HCl) solution. The $CuCl_2$ is a yellow-brown solid usually sold in its hydrated state ($CuCl_2.2H_20$) with a blue-green colour. The tank holds an electrical heater used to maintain the solution at a desired temperature and an air distributor causing air bubbles to spread along in the tank. Cokir [1] defined etching as a controlled non-traditional machinery corrosion process to manufacture geometrically complex machine parts from thin and flat streets. This process is used extensively to manufacture printed circuit boards.

[1] O. Cokir. Copper etching with cupric chloride and regeneration of waste etchant. J. Matter Process Tech, 175 : 63 - 68, 2006.

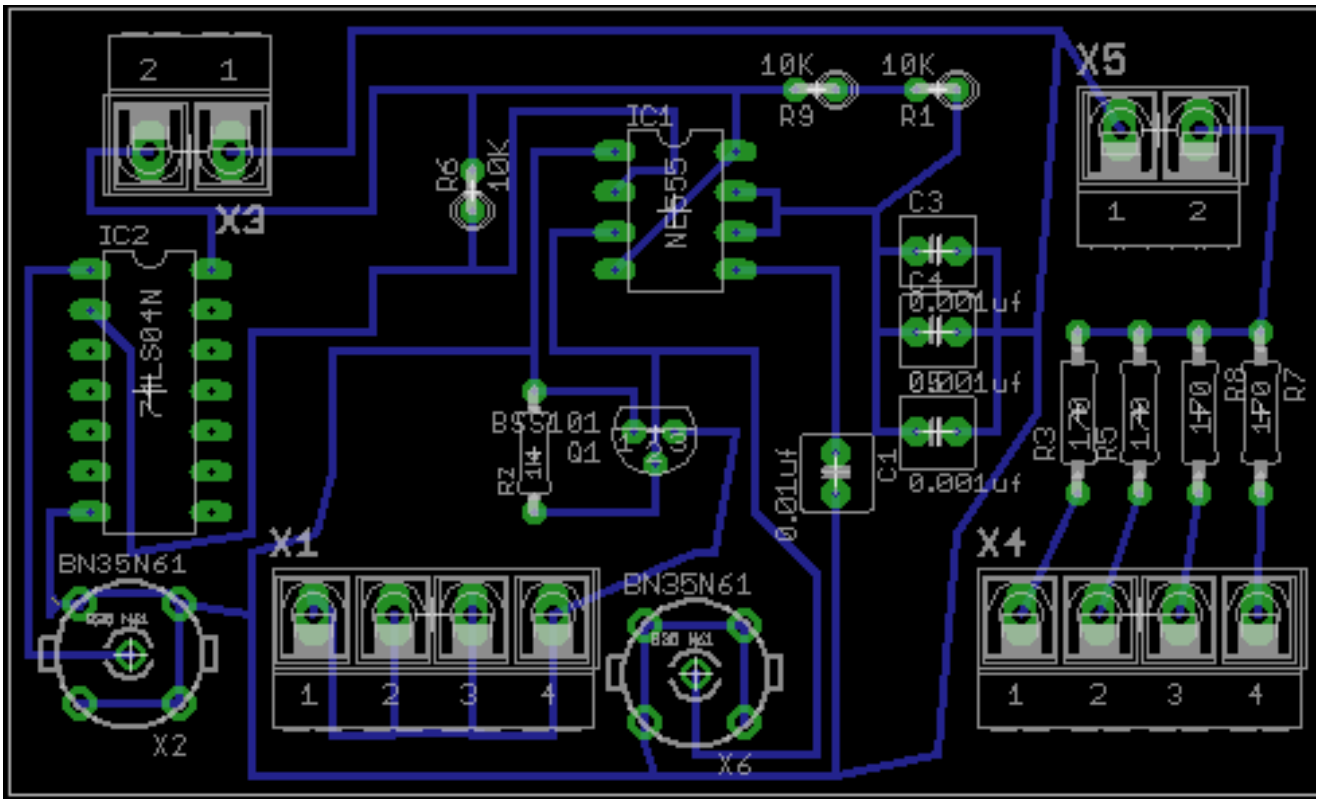

Figure A.5: A single-sided layer board showing the etched pulsing circuitry.

Appendix B

Operation manual

Figure B.1 shows the front view of the pulsing system whereas Figure B.2 shows the back view of the pulsing system.

Figure B.1: Front view of the pulsing system.

Figure B.2: Back view of the pulsing system.

B.1 System connection

The pulsing system has five ports on the outer casing labelled 1, 2, 3, 4 and 5. Three of the ports are at the back of the case as shown in Figure B.3(a) and the other two are at the front of the case as shown in Figure B.3(b). The ports are for the following: LED connectors, positive and negative (1 and 2), input-trigger from the multichannel scaler (3), output pulse (4) and a power connector (5).

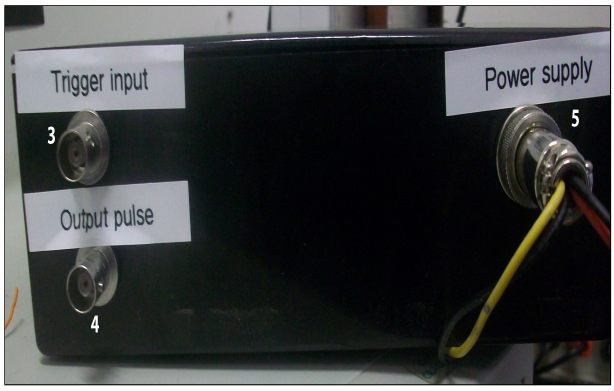

(a)

(b)

Figure B.3: The pulsing system showing five ports on the case. The back view of the pulsing system shows the input trigger, output pulse and power supply connecting ports (a) the front view of the pulsing system shows the positive and negative LED connecting ports (b).

B.1.1 Connecting the system to power supply

The pulsing system needs two different types of input voltage as identified by the colour of two different cables as shown in Figure B.4. The red cable is connected to a 5 - 15 V power supply and the yellow cable is connected to a 3 - 17 V power supply. However, the recommended input voltage for the red cable is 5 V while the yellow cable can be varied between 3 and 17 V where control of power of the stimulating light source is required. The red cable supplies input voltage to the NE555N timer and the yellow cable supplies voltage to the LED.

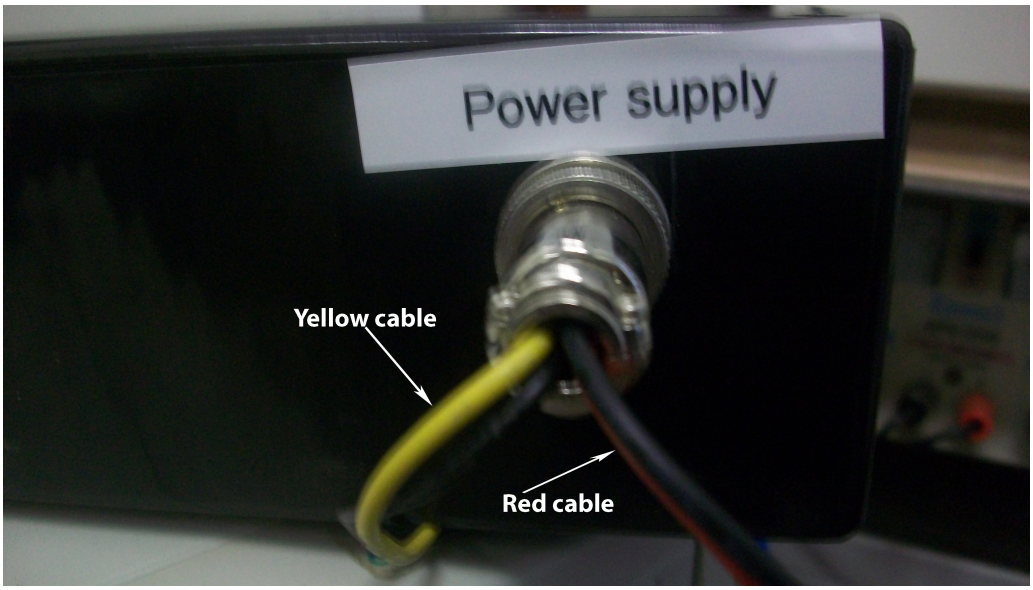

Figure B.4: A diagram showing the pulsing system power supply.

B.1.2 Connecting the system to a multichannel scaler

The multichannel scaler card is inserted into a computer. The cable from the multichannel scaler port has to be connected to the input-trigger port at the back of the case of the pulsing system.

B.1.3 Connecting system output signal to an oscilloscope

An oscilloscope is used to monitor the output waveform of the pulsing system by connecting to the output-pulse port at the back of the case of the pulsing system.

B.1.4 Connecting light-emitting-diodes

The light-emitting-diodes are arranged in a dural holder connected in parallel in sets of four each containing four LEDs in serial. We used a dural holder already available in our laboratory. Figure B.5 shows a dural holder and a metal attachment constructed to hold the Schott GG-420 filter. Figure B.5(a) shows a dural holder containing the 16 LEDs. The cable from the dural holder is connected to the two LED-connecting ports on the front of the pulsing system. The cable has two connecting heads, one is for the LED positive connector port while the other is connected to the LEDs negative port. As a means of safety, the cable heads were designed to fit into only one port.

Figure B.5(b) shows a constructed circular metal that holds the Schott GG-420 long-pass filter. To remove the filter, slowly pull out the filter out of the circular metal holder. Figure B.6 shows how to place the dural holder containing the 16 LEDs onto the circular metal holder with the Schott GG-420 filter.

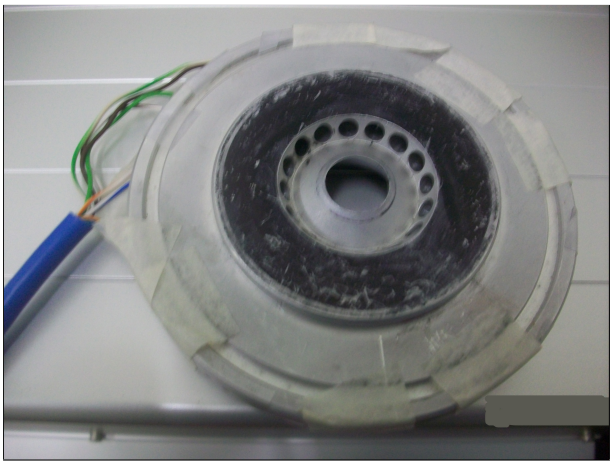

(a)

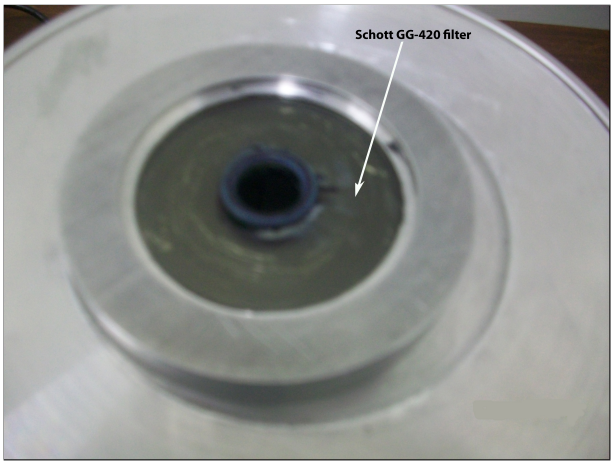

(b)

Figure B.5: A dural holder containing the 16 LEDs (a) and a Schott GG-420 filter placed inside a circular metal carrier (b).

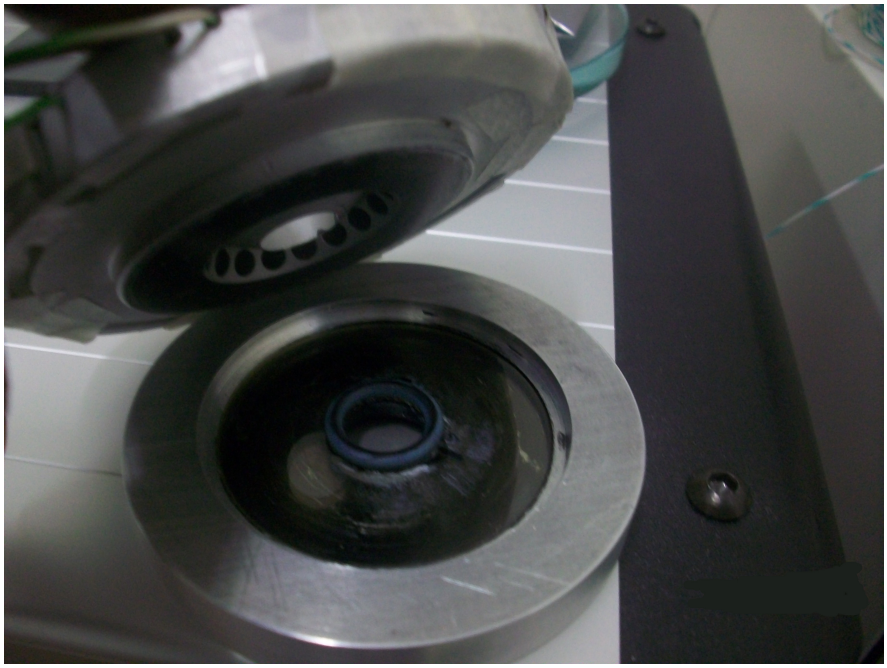

Figure B.6: Placing the dural holder containing the 16 LEDs on the circular metal carrier which contains the Schott GG-420 filter.